Available online at www.sciencedirect.com
SCIENCE DIRECT®
Materials Chemistry and Physics 92 (2005) 572–577
MATERIALS CHEMISTRY AND PHYSICS
www.elsevier.com/locate/matchemphys

Study of cobalt dispersion on titania consisting various rutile: anatase ratios

Bunjerd Jongsomjit*, Tipnapa Wongsalee, Piyasan Praserthdam

Center of Excellence on Catalysis and Catalytic Reaction Engineering, Department of Chemical Engineering, Faculty of Engineering, Chulalongkorn University, Bangkok 10330, Thailand

Received 29 October 2004; received in revised form 25 January 2005; accepted 16 February 2005

Abstract

The number of reduced cobalt metal surface atoms in Co/TiO_2 was found to increase with the presence of rutile phase. It was suggested that the increased number of reduced cobalt metal surface atoms be attributed to highly dispersed cobalt oxide species as seen by the transmission electron microscopy (TEM) technique. Besides the dispersion of cobalt oxide species, it should be noted that the presence of rutile phase in titania could facilitate the reduction of highly dispersed cobalt oxides species into the reduced cobalt metal surface atoms. It was concluded that both highly dispersed cobalt oxide species and the presence of rutile phase could result in the large number of reduced cobalt metal surface atoms.

Keywords: Titania; Cobalt; Catalyst; TEM; Chemisorption

1. Introduction

Inorganic materials such as silica (SiO_2), alumina (Al_2O_3), and titania (TiO_2) are commonly used as a carrier or support for catalytic materials due to their high surface areas, high thermal stability and high mechanical resistance. Thus, an active catalytic phase such as metal or metal oxide species can be highly dispersed on the high surface area supports. It is noted that high dispersion of the active catalytic phase may lead to great accessibility to utilize the active sites for surface reaction. Supported cobalt (Co) catalysts are preferred for Fischer–Tropsch synthesis (FTS) based on natural gas [1] due to their high activities for FTS, high selectivity for long chain hydrocarbons and low activities for the competitive water–gas shift (WGS) reaction [2,3]. Many inorganic supports such as silica [4–8], alumina [9–14], titania [15–17] and zeolites [18] have been extensively studied for supported Co catalysts for years. It is known that in general, the catalytic properties depend on reaction conditions, catalyst composition, type of inorganic support and the degree of metal dispersion as well.

It is reported that during the past decades, titania-supported Co catalysts have been investigated widely by many authors, especially for the application of FTS in a continuously stirred tank reactor (CSTR) [15–17]. However, it should be noted that titania itself has different crystalline phases such as anatase, brookite and rutile phase. Thus, the differences in compositions of crystalline phases could result in changes on physical and chemical properties of titania, then consequently for the dispersion of cobalt. In order to give a better understanding of those, the focus of this present study was to investigate the cobalt dispersion on titania consisting various ratios of rutile:anatase. The Co/TiO_2 was prepared and then characterized using different characterization techniques.

2. Experimental

2.1. Material preparation

2.1.1. Preparation of titania support consisting various rutile:anatase ratios

The various ratios of rutile:anatase in titania support were obtained by calcination of pure anatase titania (obtained from

* Corresponding author. Tel.: +66 2 2186869; fax: +66 2 2186766.
E-mail address: bunjerd.j@chula.ac.th (B. Jongsomjit).

0254-0584/$ – see front matter © 2005 Elsevier B.V. All rights reserved.
doi:10.1016/j.matchemphys.2005.02.016

Ishihara Sangyo, Japan) in air at temperatures between 800 and 1000 °C for 4 h. The high space velocity of air flow (16,000 h^{-1}) insured the gradual phase transformation to avoid rapid sintering of samples. The ratios of rutile:anatase were determined by XRD according to the method described by Jung et al. [19] as follows:

$$\%\text{Rutile} = \frac{1}{\left[\left(\frac{A}{R}\right)0.884 + 1\right]} \times 100$$

where, A and R are the peak area for major anatase ($2\theta = 25°$) and rutile phase ($2\theta = 28°$), respectively.

2.1.2. Preparation of Co/TiO_2 samples

A 20 wt.% of Co/TiO_2 was prepared by the incipient wetness impregnation. A designed amount of cobalt nitrate [$Co(NO_3)\cdot 6H_2O$] was dissolved in deionized water and then impregnated onto TiO_2 containing various ratios of rutile:anatase obtained from Section 2.1.1. The sample was dried at 110 °C for 12 h and calcined in air at 500 °C for 4 h.

2.2. Nomenclature

The nomenclature used for Co/TiO_2 samples in this study is following:

- Rn: titania support consisting *n*% of rutile phase (R);
- Co/Rn: titania support containing *n*% of rutile phase (R)-supported cobalt.

2.3. Characterization

2.3.1. BET surface area

BET surface area of the samples with various rutile:anatase ratios of titania was performed to determine if the total surface area changes. It was determined using N_2 adsorption at 77 K in a Micromeritics ASAP 2010.

2.3.2. X-ray diffraction

XRD was performed to determine the bulk crystalline phases of samples. It was conducted using a SIEMENS D-5000 X-ray diffractometer with Cu Kα (λ = 1.54439 Å). The spectra were scanned at a rate of 2.4° min^{-1} in the range $2\theta = 20$–80°.

2.3.3. Scanning electron microscopy and energy dispersive X-ray spectroscopy

SEM and EDX were used to determine the sample morphologies and elemental distribution throughout the sample granules, respectively. The SEM of JEOL model JSM-5800LV was applied. EDX was performed using Link Isis series 300 program.

2.3.4. Hydrogen chemisorption

Static H_2 chemisorption at 100 °C on the reduced samples was used to determine the number of reduced surface cobalt metal atoms. This is related to the overall activity of the samples during CO hydrogenation. Gas volumetric chemisorption at 100 °C was performed using the method described by Reuel and Bartholomew [20]. The experiment was performed in a Micromeritics ASAP 2010 using ASAP 2010C V3.00 software.

2.3.5. Transmission electron microscopy (TEM)

The dispersion of cobalt oxide species on the titania supports were determined using a JEOL-TEM 200CX transmission electron spectroscopy operated at 100 kV with 100 k magnification.

3. Results and discussion

The present study focused on investigation of cobalt dispersion on titania consisting various ratios of rutile:anatase. After calcination of the pure anatase titania under calcination temperatures ranged between 800 and 1000 °C for 4 h, the phase transformation from anatase to rutile phase in titania technically occurred. The amounts of rutile phase formed during calcination depend on temperatures used. The high space velocity of the air flow at 16,000 h^{-1} was applied during the calcination process in order to minimize the rapid sintering due to the phase transformation of titania. It was found that after calcination of the pure anatase sample, the amounts of rutile phase obtained ranged between 3 and 99%. The titania supports containing rutile phase of ca. 0, 3, 19, 40, 96, and 99% were named as R0, R3, R19, R40, R96, and R99, respectively. The surface areas of titania containing various rutile:anatase ratios essentially decreased from 70 $m^2\ g^{-1}$ for the R0 sample (pure anatase titania) to 49 $m^2\ g^{-1}$ for the R99 sample (99% rutile titania). XRD patterns of titania samples calcined at various temperatures between 800 and 1000 °C are shown in Fig. 1. For the pure anatase titania (R0), XRD peaks of the anatase phase of titania at 25° (major), 37°, 48°, 55°, 56°, 62°, 71°, and 75° were evident.

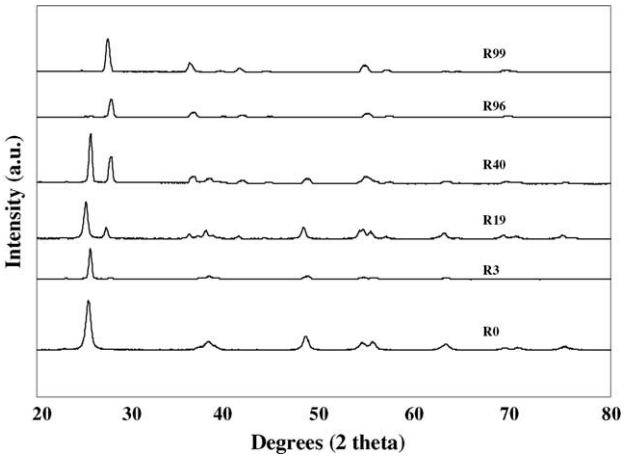

Fig. 1. XRD patterns of titania consisting various ratios of rutile:anatase phase.

After calcination of pure anatase titania sample, it was observed that besides the XRD peaks of pure anatase titania as shown above XRD peaks at 28° (major), 36°, 42°, and 57° were gradually seen. These peaks were assigned to the rutile phase essentially formed after calcination of the pure anatase titania. Apparently, the major peak at 28° of rutile phase gradually increased with increasing the calcination temperatures indicating higher content of rutile phase in titania was obtained. It was shown that the transformation from anatase to rutile phase (R99) was almost complete at temperature of ca. 1000 °C resulting in the disappearance of XRD peaks for the anatase phase of titania. After various titania supports were obtained, the preparation of Co/TiO_2 via various rutile:anatase ratios of titania was consequently conducted in order to investigate the effect of various ratios of rutile:anatase in titania supports on characteristics, especially the cobalt dispersion of Co/TiO_2.

A 20 wt.% of cobalt supported on titania consisting of various ratios of rutile:anatase phase was prepared by the conventional incipient wetness impregnation method. The XRD patterns for all calcined samples (Co/TiO_2) are shown in Fig. 2. After calcination, all calcined samples exhibited XRD peaks, which were identical with those for the corresponding titania supports. This indicated that there was no further phase transformation from anatase to rutile occurred after calcination (at temperature ca. 500 °C for 4 h) of the samples. Besides the XRD peaks of the corresponding titania supports detected, all calcined samples also exhibited weak XRD peaks at 31°, 36°, and 65°, which were assigned to the presence of Co_3O_4. However, at high content of rutile phase, the XRD peaks of Co_3O_4 were gradually diminished due to the hindrance of strong intensity of XRD peaks for the rutile phase of titania.

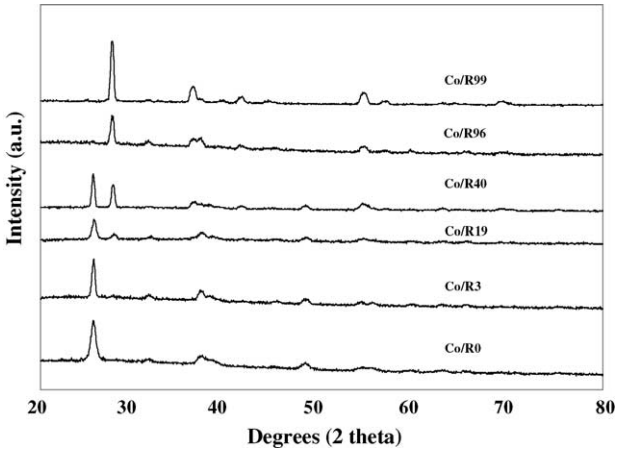

Fig. 2. XRD patterns of calcined Co/TiO_2 with various ratios of rutile:anatase phase.

Based on the XRD results, it was clear that Co_3O_4 species was definitely present in a highly dispersed form.

SEM and EDX were also conducted in order to study the morphologies and elemental distribution of the samples, respectively. Apparently, SEM micrographs and EDX mapping for all samples exhibited similar trends of morphologies and elemental (Co, Ti, and O) distributions. The typical SEM micrographs along with the EDX mapping (for Co, Ti, and O) for Co/R19 sample are illustrated in Fig. 3 indicating the external surface of the sample granule. It can be seen that the cobalt oxide species were well dispersed and distributed (shown on EDX mapping) all over the sample granule. Thus, SEM and EDX can not differentiate morphologies and elemental distributions of Co/TiO_2 consisting of various

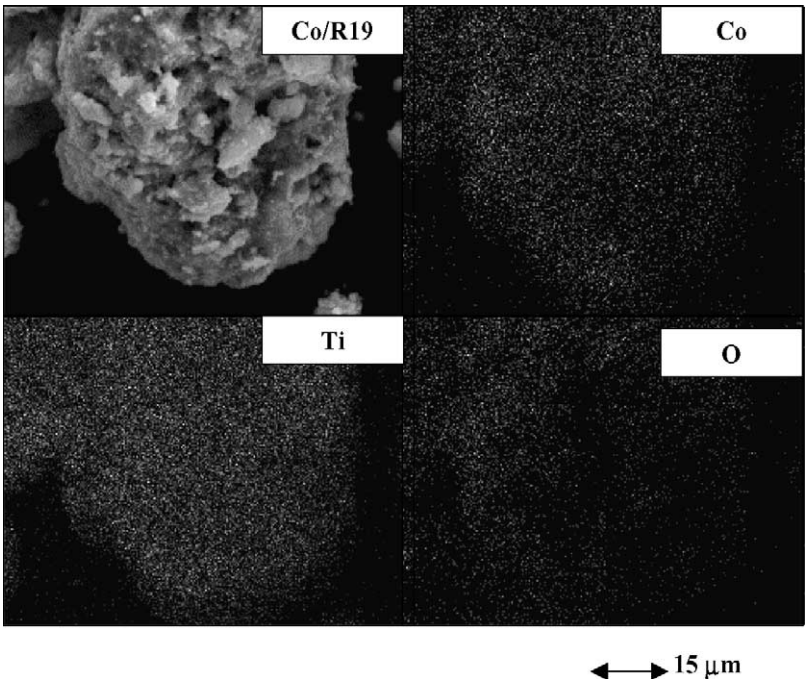

Fig. 3. SEM micrograph and EDX mapping of Co/R19 sample.

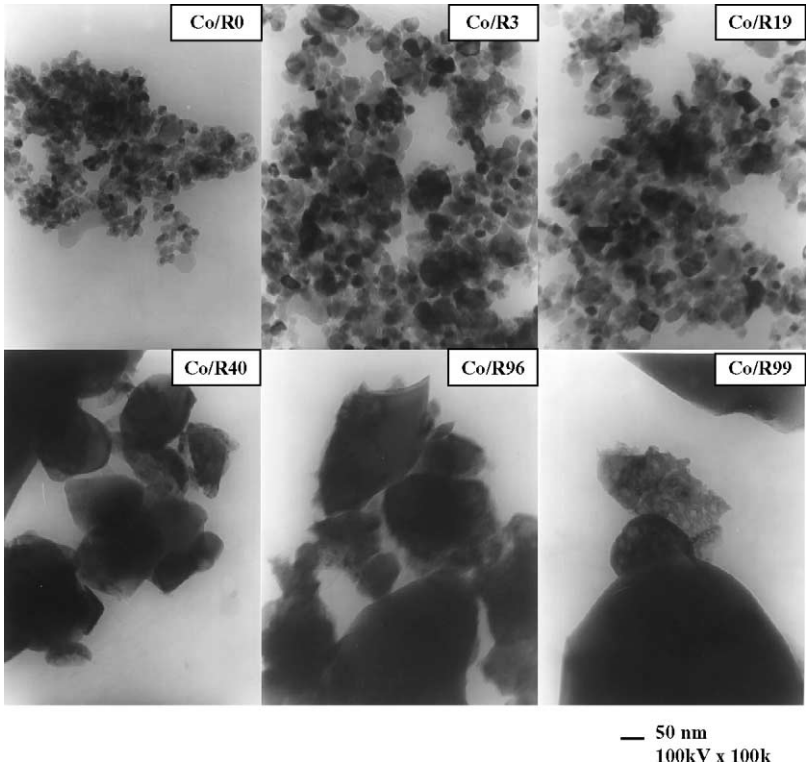

Fig. 4. TEM micrographs of Co/TiO_2 with various ratios of rutile:anatase phase.

ratios of rutile:anatase. In order to determine the dispersion of cobalt oxide species on titania, a more powerful technique such as TEM was applied to all samples. The TEM micrographs for all samples are shown in Fig. 4. The dark spots represented cobalt oxide species present after calcination of samples dispersing on titania consisting of various ratios of rutile:anatase. It can be observed that cobalt oxide species were highly dispersed on the titania supports for Co/R0, Co/R3, and Co/R19 samples resulting in an appearance of smaller cobalt oxide patches present. However, the degree of dispersion for cobalt oxide species essentially decreased with increasing the rutile phase in titania from 40 to 99% as seen for Co/R40, Co/R96, and Co/R99 samples resulting in the observation of larger cobalt oxide patches. It is suggested that the presence of the rutile phase in titania from 0 (pure anatase phase) to 19% exhibited the highly dispersed forms of cobalt oxide species for the calcined samples.

It is known that the active form of supported cobalt FTS catalysts is cobalt metal (Co^0). Thus, reduction of cobalt oxide species is essentially performed in order to transform cobalt oxide species obtained after calcination process into the active cobalt metal atoms for catalyzing the reaction. Therefore, the static H_2 chemisorption on the reduced cobalt samples was used to determine the number of reduced Co metal surface atoms. This is usually related to the overall activity of the catalyst during carbon monoxide (CO) hydrogenation. The resulted H_2 chemisorption for all samples is shown in Fig. 5. It was found that the number of the reduced cobalt metal surface atoms increased with the presence of rutile phase in titania up to a maximum at 19% of rutile phase (Co/R19) before decreasing with the greater amounts of rutile phase. Considering the number of cobalt metal atoms for Co/R0 (pure anatase titania), the number was apparently low even though highly dispersed cobalt oxides species. This was suggested that highly dispersed forms of cobalt oxide species be not only the factor that insures larger number of reduced cobalt metal surface atoms in Co/TiO_2. On the other hand, it can be observed that the number of reduced cobalt metal surface atoms for Co/R40 and Co/R96 (with the low degree of dispersion of cobalt oxide species as seen by TEM) was

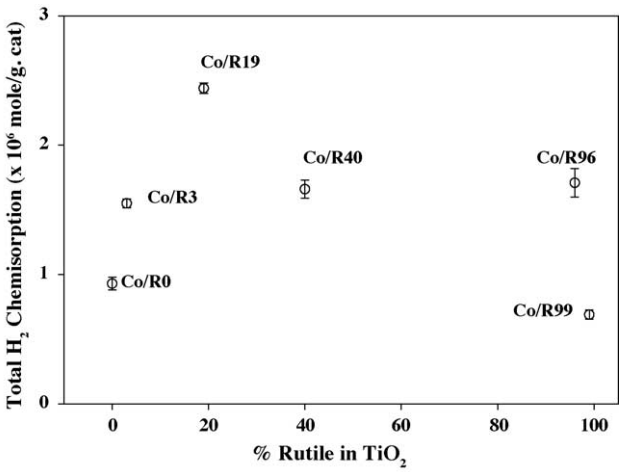

Fig. 5. A plot of the total H_2 chemisorption vs. % rutile in titania.

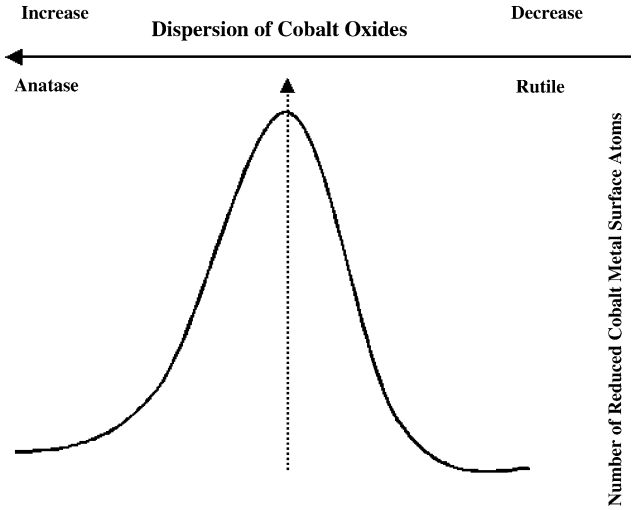

Fig. 6. A conceptual model on dependence of dispersion along with rutile phase on the number of reduced cobalt metal surface atoms for Co/TiO_2.

larger than that for Co/R0. This was due to the presence of rutile phase in Co/R40 and Co/R96. It should be mentioned that the largest number of reduced cobalt metal surface atoms for the Co/R19 sample was attributed to both highly dispersed cobalt oxide species and the presence of rutile phase in titania. In order to provide a better understanding for effects of both dispersion of cobalt oxide species and the presence of rutile phase in titania on the number of reduced cobalt metal surface atoms, a conceptual model of those is illustrated in Fig. 6. Thus, a large number of reduced cobalt metal surface atoms in Co/TiO_2 can be obtained with an optimum amount of rutile phase along with highly dispersed cobalt oxide species prior to reduction. It was suggested that the presence of rutile phase in titania can facilitate the reduction of cobalt oxide species as shown in Fig. 7. It was observed that the presence of rutile phase resulted in lowering the reduction temperature. However, the large amounts of rutile phase can result in a small number of reduced cobalt metal surface atoms. This is due to the low degree of dispersion for cobalt oxide species

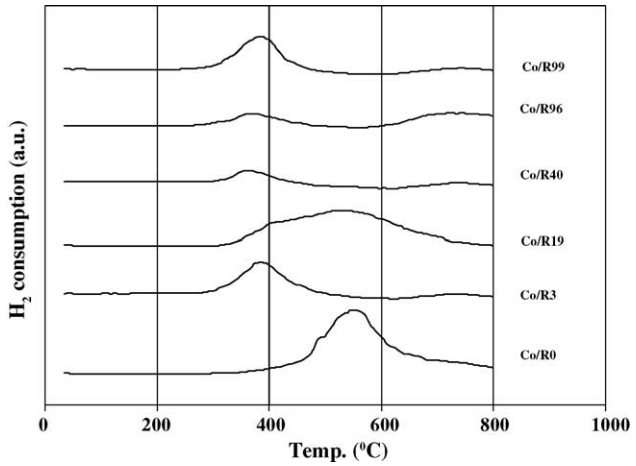

Fig. 7. TPR behaviors of Co/TiO_2 with various ratios of rutile:anatase phase.

with large amounts of rutile phase present. It should be also noted that part of the reason for the lower dispersion of Co is the lower BET surface area, especially for the rutile rich titania.

4. Conclusions

The present study showed dependence of both highly dispersed cobalt oxide species and the presence of rutile phase in titania on the number of reduced cobalt metal atoms in Co/TiO_2. It was found that the presence of rutile phase with optimum amounts in titania up to 19% resulted in highly dispersed cobalt oxide species as seen by TEM. Although with highly dispersed cobalt oxide species, Co/R0 (pure anatase titania) gave the low number of reduced cobalt metal surface atoms. On the other hand, Co/R40 and Co/R96 with a low degree of cobalt oxide dispersion apparently gave the higher number (compared to Co/Ro) of reduced cobalt metal surface atoms. Thus, both highly dispersed cobalt oxide species along with the presence of rutile phase in titania could play an important role on the number of reduced cobalt metal surface atoms for Co/TiO_2.

Acknowledgements

We gratefully acknowledge the financial support by the National Research Council of Thailand (NRCT), the Thailand Research Fund (TRF) and Thailand–Japan Technology Transfer Project (TJTTP-JBIC). We would like to thank Prof. James G. Goodwin Jr. at Clemson University for initiating this kind of project.

References

[1] H.P. Wither Jr., K.F. Eliezer, J.W. Mechell, Ind. Eng. Chem. Res. 29 (1990) 1807.
[2] E. Iglesia, Appl. Catal. A 161 (1997) 59.
[3] R.C. Brady, R.J. Pettie, J. Am. Chem. Soc. 103 (1981) 1287.
[4] A. Martinez, C. Lopez, F. Marquez, I. Duaz, J. Catal. 220 (2003) 486.
[5] J. Panpranot, J.G. Goodwin Jr., A. Sayari, Catal. Today 77 (2002) 269.
[6] J. Panpranot, J.G. Goodwin Jr., A. Sayari, J. Catal. 211 (2002) 530.
[7] S.L. Sun, I. Isubaki, K. Fujimoto, Appl. Catal. A 202 (2000) 121.
[8] S. Ali, B. Chen, J.G. Goodwin Jr., J. Catal. 157 (1995) 35.
[9] B. Jongsomjit, J. Panpranot, J.G. Goodwin Jr., J. Catal. 215 (2003) 66.
[10] T. Das, G. Jacobs, P.M. Patterson, W.A. Conner, J.L. Li, B.H. Davis, Fuel 82 (2003) 805.
[11] G. Jacobs, P.M. Patterson, Y.Q. Zhang, T. Das, J.L. Li, B.H. Davis, Appl. Catal. A 233 (2002) 215.
[12] M. Rothaemel, K.F. Hanssen, E.A. Blekkan, D. Schanke, A. Holmen, Catal. Today 38 (1997) 79.
[13] V. Ragaini, R. Carli, C.L. Bianchi, D. Lorenzetti, G. Vergani, Appl. Catal. A 139 (1996) 17.

[14] V. Ragaini, R. Carli, C.L. Bianchi, D. Lorenzetti, G. Predieri, P. Moggi, Appl. Catal. A 139 (1996) 31.
[15] J.L. Li, G. Jacobs, T. Das, B.H. Davis, Appl. Catal. A 233 (2002) 255.
[16] G. Jacobs, T. Das, Y.Q. Zhang, J.L. Li, G. Racoillet, B.H. Davis, Appl. Catal. A 233 (2002) 263.
[17] J.L. Li, L.G. Xu, R. Keogh, B.H. Davis, Catal. Lett. 70 (2000) 127.
[18] X.H. Li, K. Asami, M.F. Luo, K. Michiki, N. Tsubaki, K. Fujimoto, Catal. Today 84 (2003) 59.
[19] K.Y. Jung, S.B. Park, J. Photochem. Photobio. A: Chem. 127 (1999) 117.
[20] R.C. Reuel, C.H. Bartholomew, J. Catal. 85 (1984) 63.

Molecules **2005**, *10*, 672-678

molecules

ISSN 1420-3049
http://www.mdpi.org

Catalytic Activity During Copolymerization of Ethylene and 1-Hexene via Mixed TiO_2/SiO_2-Supported MAO with *rac*-$Et[Ind]_2ZrCl_2$ Metallocene Catalyst

Bunjerd Jongsomjit*, Sutti Ngamposri and Piyasan Praserthdam

Center of Excellence on Catalysis and Catalytic Reaction Engineering, Department of Chemical Engineering, Faculty of Engineering, Chulalongkorn University, Bangkok 10330 Thailand, Phone: (+66) 2-2186869, Fax: (+66) 2-2186766

*To whom all correspondence should be sent; e-mail: bunjerd.j@chula.ac.th

Received: 07 October 2004 / Accepted: 16 November 2004 / Published: 14 July 2005

Abstract: Activities during ethylene/1-hexene copolymerization were found to increase using the mixed titania/silica-supported MAO with *rac*-$Et[Ind]_2ZrCl_2$ metallocene catalyst. Energy Dispersive X-ray spectorcopy (EDX) indicated that the titania was apparently located on the outer surface of silica and acted as a spacer to anchor MAO to the silica surface. IR spectra revealed the Si-O-Ti stretching at 980 cm^{-1} with low content of titania. The presence of anchored titania resulted in less steric hindrance and less interaction due to supporting effect.

Keywords: Metallocene catalyst, titania, silica, supports, copolymerization

Introduction

Commercial interest in using metallocene catalysts for olefin polymerization has brought about an extensive effort towards utilizing metallocene catalysts more efficiently. It is known that the copolymerization of ethylene with higher 1-olefins is of commercial importance for production of elastomers and linear low-density polyethylene (LLDPE). Metallocene catalysts with MAO have been studied for such a copolymerization. In fact, zirconocene catalysts along with MAO have been reported to be potentially useful for polymerizing ethylene with 1-olefins [1-2].

However, it was found that homogeneous metallocene catalytic systems have two major disadvantages; the lack of morphology control of polymers produced and reactor fouling. Therefore, binding these metallocene catalysts onto inorganic supports can provide a promising way to overcome these drawbacks. Many inorganic supports such as SiO_2, Al_2O_3 and $MgCl_2$ have been extensively studied for this purpose [3-13]. Silica is perhaps the most widely used support for metallocene catalysts so far, but the properties of SiO_2 itself may not be completely satisfactory for all purposes based on activities and quality of polymer produced. For instance, it was found that the activity of the heterogeneous system was lower compared to the homogeneous one. Therefore, a modification of the support is required in order to maintain high activity. TiO_2-SiO_2 mixed oxide has been considered to be very attractive as combined catalyst and support, which have attracted much attention in recent years. It was reported that TiO_2-SiO_2 mixed materials have been used as catalysts and supports for various reactions [14]. This TiO_2-SiO_2 mixed oxide would lead to robust catalytic supports of metallocene catalysts for olefin polymerization.

In this present study, the ethylene/1-hexene copolymerization using TiO_2-SiO_2 mixed oxides supported-MAO with a zirconocene catalyst was investigated for the first time. The mixed oxide supports and catalyst precursors were prepared, characterized and tested for ethylene/1-hexene copolymerization.

Results and Discussion

The present study showed the influences of titania/silica mixed oxide supports on the catalytic activities in a heterogeneous metallocene catalytic system. The mixed oxide supports containing various amounts of titania and silica were characterized. It was found that at low concentrations (20 to 60 wt %) of titania, the latter was apparently located on the outer surface of silica. A typical EDX (Energy Dispersive X-ray spectroscopy) mapping for the cross sectional area of the mixed oxide support containing low concentrations of titania is shown in Figure 1, indicating the location of titania on the outer surface of silica. However, it can be observed that with high concentrations of titania, it started to segregate from silica probably due to its adsorption ability.

Figure 1. A typical EDX mapping of titania/silica mixed oxide support at low concentrations of titania.

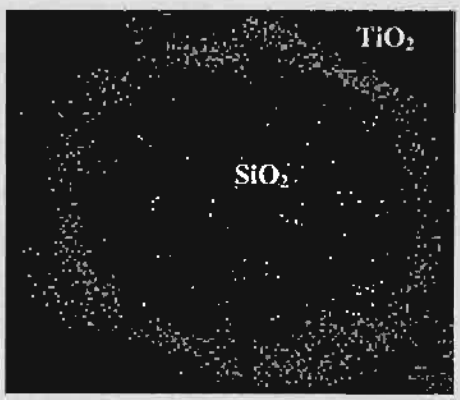

IR spectroscopy was also performed in order to identify chemical species and bonding of the mixed oxide supports. The IR spectra of samples are shown in Figure 2. It revealed that at low

concentrations of titania, the IR band at ca. 980 cm^{-1} assigning to Si-O-Ti connectivity was observed as also reported by Dutoit *et al.* [15]. This indicated that the Si-O-Ti bond was formed at the titania/silica ratios of 20/80 and 40/60 suggesting an anchor or a spacer effect. Strong IR bands were also seen at ca. 1100 cm^{-1} and assigned to asymmetric Si-O-Si stretching vibration.

Figure 2. IR spectra of titania/silica mixed oxide supports

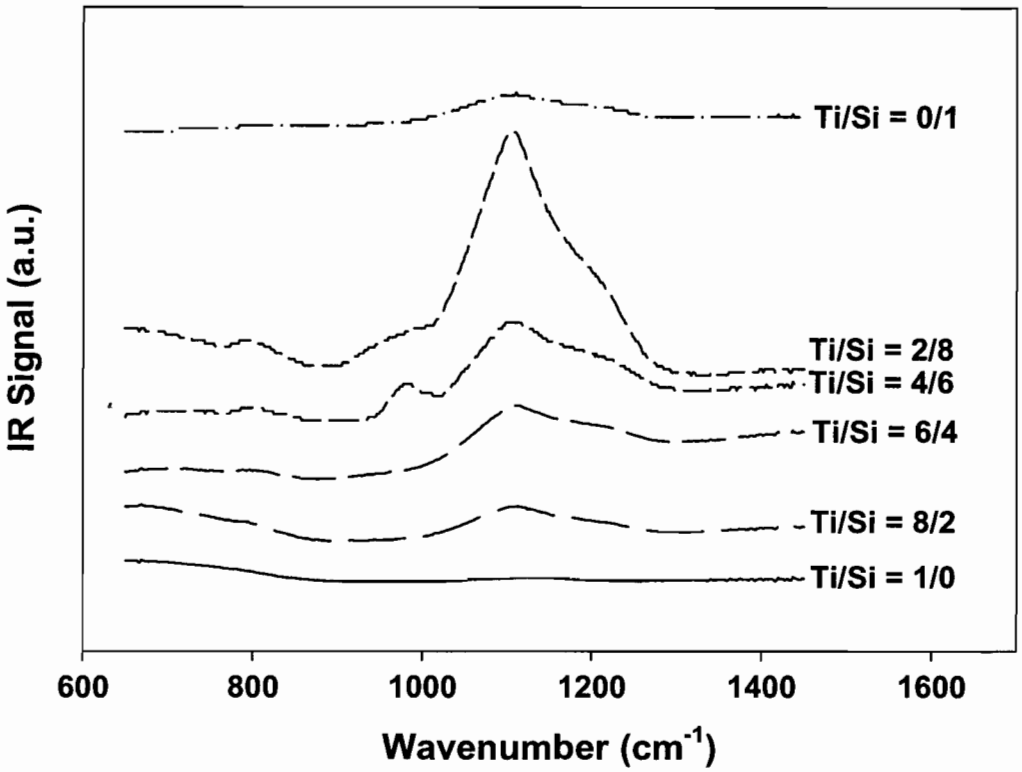

Copolymerization of ethylene/1-hexene via various titania/silica mixed oxides-supported MAO with a zirconocene catalyst was performed in order to determine the catalytic activities influenced by the various supports. The resulting reaction study is shown in Table 1 and Figure 3. The activities of the supported system were much lower than the homogeneous one, as expected. However, considering only the supported system, it was found that activities increased with increasing the amounts of titania up to 60% in the supports. The maximum activity can be obtained with the presence of 20% titania in the mixed support. However, increasing the amounts of titania more than 60% resulted in lower activities compared to the pure silica. It was also found that the activity for the pure titania is the lowest due to the strong support interaction between MAO and titania. Thus, due to the strong support interaction, it was more difficult for MAO to be released from the surface and reacted with the catalyst resulting in a low activity. Based on the resulted activities, the role of titania in titania/silica mixed oxide supports can be proposed.

Table 1: Catalytic activities during ethylene/1-hexene copolymerization via TiO_2-SiO_2 mixed oxides supported-MAO with zirconocene catalyst

TiO_2-SiO_2 Weight Ratios	wt% of TiO_2 in Mixed Support	Polymer Yield[a] (g)	Polymerization time (s)	Catalytic Activity[b] (x 10^{-4} kg polymer/mol Zr · h)
homogeneous	0	1.13	81	3.4
0/100	0	1.19	148	1.9
20/80	20	1.16	109	2.6
40/60	40	1.18	128	2.2
60/40	60	1.17	142	2.0
80/20	80	1.15	151	1.8
100/0	100	1.16	165	1.7

[a] The polymer yield was fixed [limited by ethylene fed and 1-hexene used (0.018 mole equally)]

[b] Activities were measured at polymerization temperature of 70°C, [ethylene] = 0.018 mole, [1-hexene] = 0.018 mole, $[Al]_{MAO}/[Zr]$ 1135, $[Al]_{TMA}/[Zr]$ = 2500, in toluene with total volume = 30 ml, and [Zr] = 5 x 10^{-5} M.

Figure 3. Activities of EH copolymerization via various mixed oxides-supported MAO and homogeneous system.

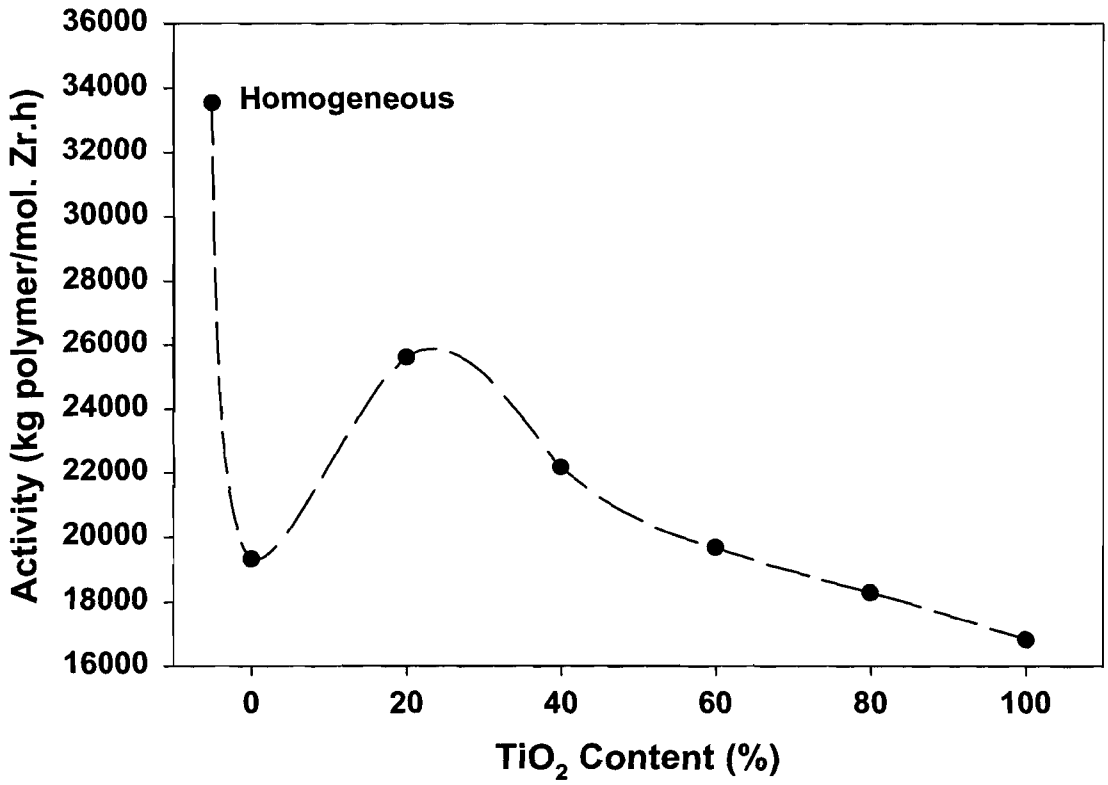

In order to give a better understanding for the role of titania, a conceptual model for titania effect is illustrated in Scheme 1.

Scheme 1 Suggested conceptual model as a spacer of titania

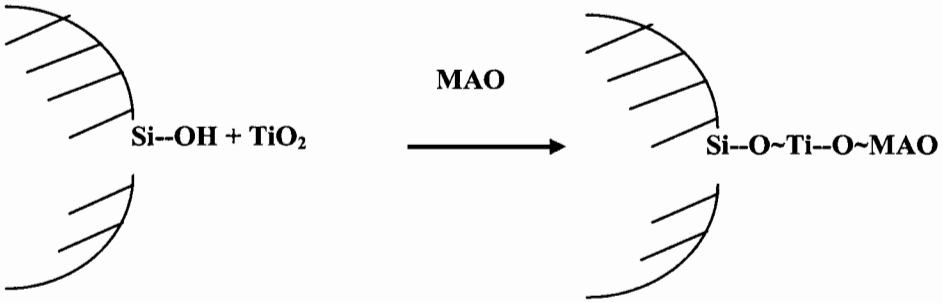

As known, when the supported system was conducted, activities decreased significantly compared to the homogeneous one. This should be due to a loss of active species by support interaction and/or the steric hindrance arising from the support. It can be observed that activities on the supported system can be divided into three levels; (i) moderate activity with the pure silica support, (ii) high activity with the certain amounts of titania present in the mixed oxide support, (iii) low activity with the pure titania support (due to strong support interaction). In Scheme 1, it showed that the presence of certain amounts (20 to 60 wt%) of titania enhanced activities. The contribution of titania can be drawn as MAO anchored on silica with titania as a spacer group. It can be also seen from SEM and EDX mapping that at low content, titania was decorated on silica surface and acted as a spacer to anchor MAO to the silica support. Thus, activities increased up to 30% with the presence of titania between 20 and 40 wt% in the mixed oxide supports. It should be mentioned that increased activities with the presence of titania as a spacer were observed because of less steric hindrance and less interaction on the support surface when a spacer was introduced. On the other hand, titania present would result in more homogeneous-like in terms of activities obtained. Investigation of a spacer such as silane in copolymerization of ethylene/1-olefins was also reported [16, 17]. However, when high amounts of titania were added, activities decreased because of the strong support interaction in titania compared to silica. Morphologies of polymers (not shown) produced via various supports were also investigated. It indicated that there was no significant change in polymer morphologies upon various mixed oxide supports used. Other characteristics of polymers produced need to be further investigated for future work.

Conclusions

The present study revealed influence of various titania/silica mixed oxides-supported MAO on the catalytic activities during copolymerization of ethylene/1-hexene with a zirconocene catalyst. It was found that with certain contents of titania ranged between 20 and 40 wt% in the mixed oxide supports, activities essentially increased up to 30% compared to one with the pure silica. It was proposed that titania added acted as a spacer to anchor MAO to the silica support resulting in less steric hindrance and less interaction on the support surface. On the other hand, titania present led to a more homogeneous-like catalytic system. However, larger amounts of titania resulted in lower activities due to the strong support interaction.

Acknowledgments

The authors would like to thank the Thailand Research Fund (TRF), National Research Council of Thailand (NRCT) and Thailand-Japan Transfer Technology Project (TJTTP-JBIC) for the financial support of this work.

Experimental

General

All chemicals [TiO_2 (anatase, Ishihara), SiO_2 (Cariact P-10), toluene, rac-ethylenebis(indenyl) zirconium dichloride [$Et(Ind)_2ZrCl_2$], methylaluminoxane (MAO), trimethylaluminum (TMA) and 1-hexene] were manipulated under an inert atmosphere using a vacuum glove box and/or Schelenk techniques.

Preparation of TiO_2-SiO_2 mixed oxides support

TiO_2-SiO_2 mixed oxide supports [surface areas of SiO_2 = 300 m^2/g and TiO_2 (anatase form) = 70 m^2/g] for MAO were prepared according to the method described by Conway *et al.* [18]. The TiO_2: SiO_2 ratios were varied from 0:1, 2:8, 4:6, 6:4, 8:2, and 1:0. The supports were heated under vacuum at 400°C for 6 h.

Preparation of TiO_2-SiO_2 mixed oxides-supported MAO

The TiO_2-SiO_2 mixed oxide support obtained above (1 g) was reacted with the desired amount of MAO at room temperature and stirred for 30 min. The solvent was then removed from the mixture. About 20 mL of toluene was added into the obtained precipitate, stirred the mixture for 5 min, and then removed the solvent. This procedure was done for 5 times to ensure the removal of impurities. Then, the solid part was dried under vacuum at room temperature to obtain white powder of TiO_2-SiO_2 mixed oxides-supported MAO.

Polymerization Reaction

The ethylene/1-hexene copolymerization reaction was carried out in a 100 mL semi-batch stainless steel autoclave reactor equipped with a magnetic stirrer. At first, the supported MAO (0.1 g, $[Al]_{MAO}/[Zr]$ = 1135) and 1-hexene (0.018 mole) along with toluene (to make the total volume of 30 mL) were put into the reactor. The desired amount of $Et(Ind)_2ZrCl_2$ (5×10^{-5}M) and TMA ($[Al]_{TMA}/[Zr]$ = 2500) was mixed and stirred for 5-min aging at room temperature, separately, then was injected into the reactor. The reactor was frozen in liquid nitrogen to stop reaction for 15 min and then the reactor was evacuated to remove argon. The reactor was heated up to polymerization temperature (70°C). To start the reaction, ethylene (0.018 mole) was fed into the reactor containing the comonomer and catalyst mixtures. After all ethylene was consumed, the reaction was terminated by addition of acidic

methanol (0.1% HCl in methanol) and stirred for 30 min. After filtration, the obtained copolymer (white powder) was washed with methanol and dried at room temperature.

Characterization of supports and catalyst precursors

Scanning Electron Microscopy and Energy Dispersive X-ray spectroscopy: SEM and EDX were used to determine the sample morphologies and elemental distribution throughout the sample granules, respectively. The JEOL model JSM-5800LV SEM was applied to determine morphologies of polymers. EDX was performed using Link Isis series 300 program. EDX is used to determine an elemental distribution as a density mapping of the specified element. Thus, it can reveal which elements are present and where they are located.

FTIR spectroscopy: FTIR was conducted on a Perkin-Elmer series 2000 instruments. The supports (1 mg) were mixed with 100 mg dried KBr. The sample cell was purged with oxygen. About 400 scans were accumulated for each spectrum in transmission with a resolution of 4 cm^{-1}. The spectrum of dried KBr was used as a background subtraction.

References

[1] Shan, C.L.P.; Soares, J.B.P.; Penlidis, A. *Polym. Chemistry* **2002**, *40*, 4426.
[2] Chu, K.J.; Shan, C.L.P.; Soares, J.B.P.; Penlidis, A. *Macromol. Chem. Phys.* **1999**, *200*, 2372.
[3] Uusitalo, A.M.; Pakkanen, T.T.; Iskola, E.I. *J. Mol. Catal. A: Chem.* **2002**, *177*, 179.
[4] Soga K.; Kaminaka, M. *Makromol. Chem.* **1993**, *194*, 1745.
[5] Ko, Y.S.; Han, T.K.; Park, J.W.; Woo, S.I. *Macromol. Rapid Commun.* **1996**, *17*, 749.
[6] Sugano T.; Yamamoto, K. *Eur. Pat. Appl.* 728773, **1996**.
[7] Margue M.; Conte, A. *J. Appl. Polm. Sci.* **2002**, *86*, 2054.
[8] Sensarma S.; Sivaram, S. *Polym Inter.* **2002**, *51*, 417.
[9] Belelli, P.G.; Ferreira M.L.; Damiani, D.E. *Appl.Catal. A: Gen.* **2002**, *228*, 189.
[10] Xu, J.T.; Zhu, Y.B.; Fan, Z.Q.; Feng, L.X. *J. Polym. Sci. Part A: Polym Chem.* **2001**, *39*, 3294.
[11] Korach L.; Czaja, K. *Polym. Bull.* **2001**, *46*, 67.
[12] Koppl A.; Alt, H.G. *J. Mol. Catal.A: Chem.* **2001**, *165*, 23.
[13] Jongsomjit, B.; Praserthdam, P.; Kaewkrajang, P. *Mater. Chem. Phys.* **2004**, *86*, 243.
[14] Gao X.; Wachs, I.E. *Catal. Today* **1999**, *51*, 233.
[15] Dutoit, D.C.M.; Schneider, M.; Baiker, A. *J. Catal.* **1995**, *153*, 165.
[16] Chao, C.; Pratchayawutthirat W.; Praserthdam, P.; Shiono T.; Rempel, G.L. *Macromol. Rapid Commun.* **2002**, *23*, 672.
[17] Jongsomjit, B.; Kaewkrajang, P.; Wanke, S.E.; Praserthdam, P. *Catal. Lett.* **2004**, *94*, 205.
[18] Conway, S.J.; Falconer, J.W.; Rochester, C.H. *J. Chem. Soc. Faraday Trans.* **1989**, *85*, 71.

Samples Availability: Available from the authors.

Korean J. Chem. Eng., 22(1), 115-120 (2005)

New Concepts in Material and Energy Utilization

Piyasan Praserthdam†, Choowong Chaisuk*, Wilasinee Kongsuebchart, Supakanok Thongyai and Sirachaya Kunjara Na Ayudhya

Center of Excellence on Catalysis and Catalytic Reaction Engineering,
Department of Chemical Engineering, Chulalongkorn University, Bangkok 10330, Thailand
*Department of Chemical Engineering, Silpakorn University,
Sanam Chandra Palace Campus, Nakorn Pathom 73000, Thailand
(*Received 13 July 2004 • accepted 15 October 2004*)

Abstract–New criteria in material and energy utilization are proposed. The potential index (Θ^*) is assigned to explain some natural processes in the world and to identify reasonably the preferable process instead of the efficiency. In addition, this term can first integrate the independent knowledge of the fields of mechanical, electrical and chemical engineering. It not only describes satisfactorily the transformation processes that are well-known in mechanical and electrical engineering, but also the increasing potential processes familiar in chemical engineering.

Key words: Material, Energy, Utilization, Potential, Potential Index

INTRODUCTION

In the beginning, chemical engineering originated by developing and applying the law of conservation of material, momentum and energy to explain simple phenomena in industrial processes. This was concerned with fundamentally designing equipment and operating processes well-known as "unit operations." Also, this knowledge was dramatically extended to a benign environmental approach, e.g. a waste treatment process. This can only minimize negative environmental impact in downstream, but it is not enough to optimize the usage of material and energy to acquire the highest gain or the lowest loss. Subsequently, a state-of-the-art method of cleaner technology was pronounced to be a promising way to manage the material and energy, since this procedure can determine an upstream route of processes. However, there is still some doubtfulness about this because most human beings tend to regard economic profits more than long-term planning. In addition, selecting the most suitable process is a difficult decision, especially in separation processes in chemical engineering, because there is not yet an indicator for analysis and interpretation. For example, which favorable process between distillation and solvent extraction is more worthy of the utilization of material and energy. On the contrary, most processes of energy transformation for mechanical and electrical engineering can be reliably altered by using the efficiency (η). Because of this we cannot point out the best direction of research and development in future. As mentioned above, we intend to propose a new approach to manage, utilize and optimize material and energy coincident with executive decision to select the preferable process in worldwide circumstances.

Usually in engineering work, we are familiar with the term efficiency, which is defined as the useful energy or work we want over the energy or work we have input. In addition, chemical engineers compare new process with conventional processes through the terms efficiency, conversion or recovery, which are usually defined the same as efficiency. The usage of efficiency, conversion and recovery is spread through many areas of chemical engineering such as packed bed columns [Han et al., 1985], combustion & conversion [Choi et al., 1985; Jung et al., 1988; Yun et al., 2001], distillation [Yoo et al., 1988; Kang et al., 1996], absorption [Park et al., 1990; Oh et al., 1999], fluidized beds [Kage et al., 1999; Jang, 2002] and membranes [Kang et al., 2002]. None of them can compare the processes that are different than their definition of efficiency, conversion and recovery. Most of them compared the new method in the same machine to the old process of the same machine and used it in the process design work only. That is the reason why we have proposed a new way of looking at efficiency, conversion or recovery and distributed these terms through many processes that we defined as the system and the surroundings. We have found many amazing results through the use of the potential index, as we will explain in detail as follows.

DETAILS

The basic idea of the law of conservation of mass, momentum and energy is mathematically expressed as follows [Smith et al. 2001; Jui, 1993; Van, 1959; Bird, 1960].

Rate of M.M.E. accumulation=Rate of M.M.E. generation
+Rate of M.M.E. Net I/P (1)

where M.M.E. refers to mass or momentum or energy and I/P refers to input minus output.

Eq. (1) can be applied to investigate simply mass minimization and energy preservation, but it still lacks a universal representative to evaluate and manipulate ineffective processes due to just a macroscopic approach. However, if the principle of energy interconversion and balance, which is the simplest expression of the first law of thermodynamics, is only considered, a measure of accomplishment of any processes may be definitely evaluated in terms of the efficiency (η) [Smith et al., 2001; Jui, 1993; Van, 1959] as defined:

†To whom correspondence should be addressed.
E-mail: piyasan.p@chula.ac.th

1. A process in which either material or energy is transformed is named as "Transformation Process".

2. A process in which either material or energy potentials in the system increase but no transformation is named as "Increasing Potential Process".

Mechanical and electrical engineers are interested in energy transformation processes, whereas chemical engineers have emphasized the increasing potential process, especially the separation process. Five examples of transformation of energy are shown as follows:

1. Thermal to mechanical energy.

- Carnot engine gives approximately 50% of the maximum thermal efficiency based on T_L=300 K and T_H=600 K [Smith et al., 2001; Jui, 1993; Van, 1959].
- Internal combustion engine [Heywood, 1988] shows maximum efficiency of spark ignition (SI) and direct injection (DI) as 0.30 and 0.45-0.53, respectively.

2. Mechanical to electrical energy or vice versa.

- Generator or motor has to be approximate values of efficiency in the range of 0.80-0.95 [Alexander et al., 1962; Sen, 1989].

3. Electrical to thermal energy.

- Heating element always shows 100% of the efficiency [Alexander et al., 1962; Sen, 1989].

4. Chemical to electrical energy.

- Fuel cell [Williams et al., 1966; EG & G. Services, 2002; Vielstich et al., 2003] can exhibit ideal or comparative thermal efficiency (ε_T) as defined in the following equation:

$$\varepsilon_T = \frac{\Delta G'}{\Delta H} = \varepsilon_G \cdot \frac{\Delta G}{\Delta H} \tag{10}$$

where $\varepsilon_G = \varepsilon_f$, ε_f=the free energy efficiency, ε_v=voltage efficiency and ε_c=current efficiency

Example: if the reaction is $H_2 + \frac{1}{2}O_2 \Leftrightarrow H_2O(l)$,

it will show $\Delta G^\circ = -56.69$ kcal and $\Delta H^\circ = -68.32$ kcal at 571 K.

It follows that a fuel cell with a free energy efficiency of 0.60 is as efficient as a device burning hydrogen at a thermal efficiency of

$$\varepsilon_T = 0.60 \times \left(\frac{-56.69}{-68.32}\right) = 0.50$$

5. Light to electrical energy.

- Solar cell shows average efficiency in the range of 7.5-30.5% [Green, 1998].

For all of transformations of one energy type to another, we have observed the same nature in such processes. When the input energy is transformed to the desired energy, the potential in the system relative to the input energy always decreases. The output reservoir shows lower temperature than the input one in a Carnot engine. The drop of voltage and the deceleration of angle velocity occur in motors or heaters and generators, respectively. To understand better the above idea, transformation of mass is also considered.

In every chemical reaction, the concentration of reactants is always reduced. Certainly, the decreasing potential behavior of material conversion is similar to that of energy transformation. As mentioned above, it is possible to imitate conversion as efficiency. However, the highest value of conversion will be limited by the thermodynamic equilibrium constant (K) [Octave, 1972] as defined in the following equation:

$$K = \frac{\text{concentration of products}}{\text{concentration of reactants}} \tag{11}$$

where K is dependent on reaction temperature.

The above observation leads to the following principle:

Principle 1 For the process in which material or energy is transformed into another form (transformation process), the material or energy potential in the system relative to the mass or energy input always decreases.

The first principle just explains the basic nature of all of processes, but it is not enough to indicate the explicit significance of the application to selecting exact useful processes. For processes concerned with energy conversion in mechanical and electrical engineering, it is well-known that the higher the efficiency, the better the process. For chemical reaction processes in chemical engineering, the promising process frequently shows higher conversion. Due to the familiar relationship of the efficiency, the mass conversion and the potential index, it can be implied that if the potential index of the system in whatever process is very high, such process can be preferable in practical operation. Recalling principle 1 and Eq. (7), it is clear that the drops of the material and energy potential are proportional to the increases of the potential index, and thus the preferable process exhibits much more decrease of the material or energy potential in the system. This statement is rewritten as follows:

Principle 2 For the process in which material or energy is transformed into another form (transformation process), the preferable process will show high potential index in the system relative to the mass or energy input.

The two principles are greater benefits to the field of mechanical and electrical engineering because most of the equipment in these fields involves energy transformation processes. However, in chemical engineering both principles can be powerfully useful in some situations. An example is the use of the second principle to understand better the second law of thermodynamics. This law affirms that every process proceeds in such a direction that the total entropy change associated with it is positive, the limiting value of zero being attained only by a reversible process. No process is possible for which the total entropy decreases. This can be expressed in the following mathematical statement [Cavaseno et al., 1979]:

$$\Delta S_{total} = \Delta S_{system} + \Delta S_{surroundings} \geq 0 \tag{12}$$

Attempts to relate the term of "potential index" with the entropy change (ΔS) are easily made. Considering the changes of thermal to mechanical energy in a reversible process with incompressible substances, the temperature (potential) of the reservoir is decreased from T_H to T_L. The entropy change of the system is expressed as follows [Cavaseno et al., 1979]:

$$\Delta S_{system} = \int \frac{\delta Q}{T} = \tilde{C}_P \int_{T_H}^{T_L} \frac{dT}{T} = \tilde{C}_P \ln \frac{T_L}{T_H} \tag{13}$$

where $\tilde{C}_P$=average heat capacity (J/K).

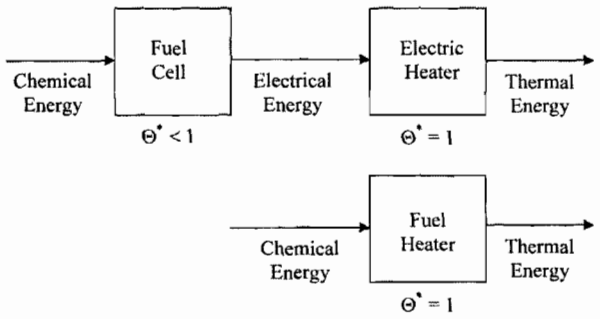

Fig. 1. Comparative process of electric and fuel heater.

From principle 2 and Eq. (13), it can be implied that a process will be great if there is much more entropy change of the system.

The two principles can briefly guide us to being careful in the operation of processes. If the potential index in the system of the transformation process is very low, such a process. Generators, motors and heaters are examples of preferable instruments because their potential indexes are normally unity. However, if there are many types of the instruments, we can select the preferable one as shown in the following example of the heater selection. At present, two main sources of heaters, electric and fuel heaters, are usually used. Both show a unity of the potential index. Nevertheless, if we focus on the same sources of the input energy, the relative difference can be obtained. This is schematically shown in Fig. 1.

Recalling principle 2, the electric heater should be avoided because there is a low potential index in the subsystem of the overall process.

Although the transformation process is very important, most of the processes in chemical engineering become the increasing potential processes, especially various separation processes. Two main examples are as follows:

1. Processes in which material potential in the system is increased.

As mentioned above, if we refer to material, the concentration will be considered as the potential and for all of these processes, the concentration increases. However, in some cases we may assign the mole fraction instead of the concentration. There are many examples in separation processes such as liquid-liquid extraction, solid-liquid extraction, crystallization, distillation, absorption, adsorption, evaporation, drying, filtration, membrane separation, centrifuge, thickener and electrochemical separation. To understand better, some of processes are investigated as follows:

• Liquid-liquid extraction (schematic diagram is shown in Fig. 2) [Herman et al., 1961; Carry, 1982; Warren et al., 1993; Seader et al., 1998; Alan, 1999; Piyasan, 1999].

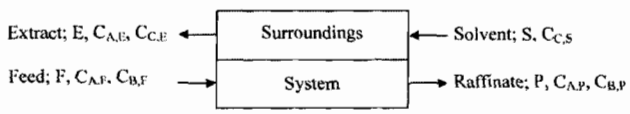

Fig. 2. Liquid-liquid extraction process: A and B=component in solute; C=solvent; F, P, S and E=volumetric flow rate (m^3s^{-1}) of feed, raffinate, solvent and extract, respectively; C_A, C_B and C_C=concentration of A, B and C (mole m^{-3}), respectively.

Basically, the process efficiency is given by recovery (R) as the following equation:

$$R = \frac{\text{A extracted}}{\text{A fed}} = \frac{FC_{A,F} - PC_{A,P}}{FC_{A,F}} \tag{14}$$

Let F=P

$$R = \frac{C_{A,F} - C_{A,P}}{C_{A,F}} = 1 - \frac{C_{A,P}}{C_{A,F}} \tag{15}$$

While

$$\Theta^*_{syst} = \frac{C_{B,P} - C_{B,F}}{C_{B,P}} = 1 - \frac{C_{B,F}}{C_{B,P}} \tag{16}$$

It is found that R and Θ^*_{syst} are quite different but still coincident. Additionally, if we just consider the surroundings, the potential index can be also expressed as follows:

$$\Theta^*_{surr} = \frac{C_{C,S} - C_{C,E}}{C_{C,S}} = 1 - \frac{C_{C,E}}{C_{C,S}} \tag{17}$$

where Θ^*_{syst}=the potential index of the system, Θ^*_{surr}=the potential index of the surroundings.

A remarkable observation is that for the extraction process if the concentration of one substance in the system is increased, the concentration of the other in the surroundings is always decreased. The "B" fraction out of the raffinate is increased, whereas the "C" fraction out of the extract is decreased.

• Binary distillation (schematic diagram is shown in Fig. 3) [Herman et al., 1961; Alan et al., 1980; Carry, 1982; Warren et al., 1993; Christie, 1993; Seader et al., 1998; Alan, 1999; Piyasan, 1999].

Again, the following recovery, potential index of the system and potential index of the surroundings are expressed:

$$R = \frac{\text{output (desired)}}{\text{Input}} = \frac{Dy_{A,D}}{Fz_{A,F}} \tag{18}$$

$$\Theta^*_{syst} = \frac{x_{C,B} - z_{C,F}}{x_{C,B}} \text{ or } \frac{y_{A,D} - z_{A,F}}{y_{A,D}} \tag{19}$$

$$\Theta^*_{surr} = \frac{T_H - T_L}{T_H} \tag{20}$$

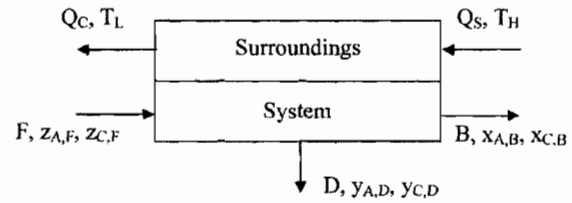

Fig. 3. Binary separation process: A and C=mixture component; F, B and D=molar flow rate (mole s^{-1}) of feed, bottom and top of distillation column, respectively; z, x and y=mole fraction in feed, bottom and top of distillation column, respectively; Q_S and Q_C=the heat flow (J s^{-1}) into reboiler and out of condenser, respectively; T_H and T_L=temperature (K) of reboiler and condenser, respectively.

The gain of potential in the system may be encountered in either the "A" component out of the top or the "C" component out of the bottom. It is clear that while "A" or "C" concentration is increased, the temperature of the bottom is higher than that of the top. This is consistent with the case of liquid-liquid extraction, but the decreasing potential term in the surroundings becomes the temperature instead of the solvent concentration.

In energy terms, potential index can be widely compared across the systems and processes similar to the term efficiency. These usually happen in case of mass terms; the potential index can be compared even with energy. In an instrument that performs similar actions such as distillation and liquid extraction, the surrounding potential index is defined as temperature in case of distillation, while the surrounding potential index is defined as concentration in the case of liquid extraction. However we can compare the potential index and select the better method according to previous or consequent processes that need to be performed in terms of potential index of the substance. The more purity of the substances, the more precious the materials.

Two examples of the processes in which material potential in the system is increased show the contradictory direction of the Θ^*_{syst} and the Θ^*_{surr}. To confirm this, we also focus on the processes in which energy potential in the system is increased.

2. Processes in which energy potential in the system is increased.

• Heat exchanger (schematic diagram is shown in Fig. 4) [Cavaseno et al., 1979; Smith et al., 2001].

A heat exchanger is a device in which energy is transferred from one fluid to another across a solid surface. The potential indexes of the system and the surroundings are shown in Eqs. (21) and (22), respectively.

$$\Theta^*_{syst} = \frac{T_H - T_L}{T_H} \tag{21}$$

$$\Theta^*_{surr} = \frac{T_{in} - T_{out}}{T_{in}} \tag{22}$$

• Pump or Compressor (schematic diagram is shown in Fig. 5)

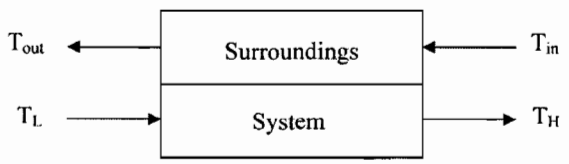

Fig. 4. Heat exchanger: T_L and T_{out}=low temperature (K), T_H and T_{in}=high temperature (K).

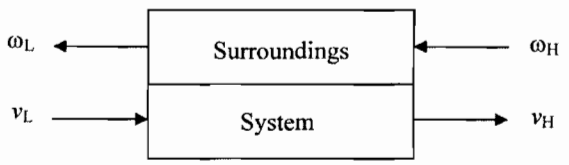

Fig. 5. Pump or compressor: v_L and v_H=liquid or gas velocity (m s^{-1}), ω_L and ω_H=angle velocity of the pump core (rpm).

[Cavaseno et al., 1979; Smith et al., 2001].

A pump is a device for moving a liquid or gas from one place to another. The potential indexes of the system and the surroundings are shown in Eqs. (23) and (24), respectively.

$$\Theta^*_{syst} = \frac{v_H - v_L}{v_H} \tag{23}$$

$$\Theta^*_{surr} = \frac{\omega_H - \omega_L}{\omega_H} \tag{24}$$

From the two examples, there is agreement with the explanation of the processes in which material potential in the systems is increased. For the heat exchanger, the temperature of the cold stream into the system is increased, whereas the temperature of the hot stream into the surroundings is decreased. For the pump or compressor, the fluid velocity into the system is increased while the angle velocity of the pump core of the surroundings is decreased. Hence, the following principle can be expressed:

Principle 3 For the process in which either material or energy potential in the system increases (increasing potential process), the material or energy potential in the surroundings always decreases.

Principle 3 is related to the second law of thermodynamics as well. From Eq. (13), the potential difference is proportional to the entropy change, and therefore the potential index can be referred to instead of the entropy change. Hence, the contradiction of ΔS_{system} and $\Delta S_{surroundings}$ in Eq, (12) implies the increases of Θ^*_{syst} coincident with the decreases of Θ^*_{surr}.

Considering some examples such as heat exchangers, a suitable heat exchanger is the one that possesses minimum mass flow rate of the substance according to economic reasons. Hence, the temperature difference, referred to as potential difference of its surroundings, is maximum. Another good example is liquid-liquid extraction. If the extract or solvent phase flow rate should be minimized, its concentration difference between input and output should consequently be high. Therefore, another principle is introduced to explain a general concept as in the above examples.

Principle 4 For the process in which either material or energy potential in the system increases (increasing potential process), if the increases of potential in the specific systems are the same, the process which shows the highest potential index in the surroundings will be preferable.

From principle 4, the calculations of liquid-liquid extraction, binary distillation and the other processes can be summarized as follows:

- Liquid-liquid extraction [Herman et al., 1961; Alan et al., 1980; Warren et al., 1993]: Θ^*_{syst} in the range of 0.080-0.530 and Θ^*_{surr} in the range of 0.120-0.595
- Binary distillation [Carry, 1982; Warren et al., 1993; Seader et al., 1998; Piyasan, 1999]: Θ^*_{syst} in the range of 0.430-0.583 and Θ^*_{surr} in the range of 0.180-0.308
- Stripping [Carry, 1982; Warren et al., 1993; Seader et al., 1998; Piyasan, 1999]: Θ^*_{syst} in the range of 0.00035-0.166 and Θ^*_{surr} in the range of 0.021-0.593
- Absorption [Alan et al., 1980; Warren et al., 1993; Shuzo, 1993;

Christie, 1993, 2003]: Θ^*_{syst} in the range of 0.012-0.196 and Θ^*_{surr} in the range of 0.0003-0.005

It is clear that if the Θ^*_{syst} of liquid-liquid extraction and binary distillation are the same, the preferable process is liquid-liquid extraction. Another observation is that if the Θ^*_{syst} of liquid-liquid extraction, stripping and absorption are the same, the preferable process becomes stripping.

The important suggestion is that whatever processes containing low potential index steps should be avoidable in operations. These are, for example, the processes involving biodiesel, gasohol, or hydrogen fuel cells. Biodiesel is produced from vegetable oil, whereas gasohol comes from ethanol. It is not worth increasing the purity of ethanol from 99.5% to 99.9% to make gasohol. Similarly, hydrogen used for fuel cells in cars is not an attractive way. These example processes are all comprised of systems of low potential index. If they are compared to other processes of fuel production such as petroleum distillation, which shows higher potential index, the latter may be more. Hence, an increase of potential index in the process is one of ways to achieve better production.

REFERENCES

Alan, J. H., *Extraction Methods in Organic Analysis*, Sheffield, England: Sheffield Academic Press, Boca Raton, FL: CRC Press (1999).

Alan, S. F., Leonard, A. W., Curtis, W. C., Louis, M. and Andersen, L. Bryce, *Principles of Unit Operations*, 2nd edition, John Wiley & Sons, Inc. (1980).

Alexander, G. and Wallace, G. A., *Principles and Practice of Electrical Engineering*, 8th edition, McGraw-Hill Book company (1962).

Atkins, P., *The Elements of Physical Chemistry*, 3rd, Oxford press (2001).

Bird, R. B., Warren, E. S. and Edwin, N. L., *Transport Phenomena*, John Wiley & Sons, INC. (1960).

Cary, J. K., *Separation Processes*, 2nd edition, New Delhi: Tata McGraw-Hill (1982).

Cavaseno, V. and the Stall of Chemical Engineering, *Process Heat Exchange*, Chemical Engineering McGraw-Hill Pub. Co. (1979).

Choi, J. H., Park, Y. S., Park, Y. O., Park, W. H. and Son, J. E., "Effect of Entrainment on Combustion Efficiency High Ash Anthracites in Fluidized Bed Combustors," *Korean J. Chem. Eng.*, **2**, 111 (1985).

Christie, J. G., *Transport Processes and Unit Operations*, 5th edition, Prentice-Hall International, Inc. (1993).

Christie, J. G., *Transport Processes and Separation Process Principles*, 4th edition, Pearson Education, Inc. (2003).

EG & G. Services, *Fuel Cell Handbook*, 5th edition, Parsons, Inc. Science Applications International Corporation (2002).

Green, M. A., "Progress in Photovoltaics, Research and Applications," **6**(1) (1998).

Han, M. W., Choi, D. K. and Lee, W. K., "Effect of Shape and Wettability of Packing Materials on the Efficiency of Packed Column," *Korean J. Chem. Eng.*, **2**, 25 (1985).

Herman, J. A., et al., *Separation Methods in Analytical Chemistry*, New York: Interscience Pub. (1961).

Heywood, J. B., *Internal Combustion Engine Fundamental*, McGraw-Hill Book Company (1988).

Jang, J. G., Kim, M. R., Lee, K. H. and Lee, J. K., "Enhancement of Combustion Efficiency with Mixing Ratio during Fluidized Bed Combustion of Anthracite and Bituminous Blended Coal," *Korean J. Chem. Eng.*, **19**, 1059 (2002).

Jui, S. H., *Engineering Thermodynamics*, Prentice-Hall, Inc. (1993).

Jung, Y. and Park, D., "Fluidized Bed Combustion of High Ash Anthracite: Analysis of Combustion Efficiency and Particle Size Distribution," *Korean J. Chem. Eng.*, **5**, 109 (1988).

Kage, H., Dohzaki, M., Ogura, H. and Matsuno, Y., "Powder Coating Efficiency of Small Particles and Their Agglomeration in Circulating Fluidized Bed," *Korean J. Chem. Eng.*, **16**, 630 (1999).

Kang, M. S., Kim, I. W. and Park, S., "Stage Efficiency Estimation by Modified MIMT Using NLP," *Korean J. Chem. Eng.*, **13**, 159 (1996).

Kang, M. S., Tanioka, A. and Moon, S. H., "Effects of Interface Hydrophilicity and Metallic Compounds on Water-Splitting Efficiency in Bipolar Membranes," *Korean J. Chem. Eng.*, **19**, 99 (2002).

Noel, D. N., *Physical and Chemical Equilibrium for Chemical Engineers*, John Wiley & Sons, Inc. (2002).

Octave, L., *Chemical Reaction Engineering*, 2nd edition, John Wiley & Sons, Inc. (1972).

Oh, E. K., Jung, G. H., Kim, S. G., Lee, H. K. and Kim, I. W., "Effect of Initial Droplet Size Distribution on Sulfur Removal Efficiency in FGD/SDA," *Korean J. Chem. Eng.*, **16**, 292 (1999).

Park, C. Y., Lee, Y. C., Chung, S. H. and Sohn, E. S., "Effect of Pore Structure on SO_2 Adsorption Efficiency," *Korean J. Chem. Eng.*, **7**, 296 (1990).

Piyasan, P., *Principles of Design Instrument for Separation*, 3th edition, cubook, Bangkok (1999).

Seader, J. D. and Ernest, J. H., *Separation Process Principles*, New York: Wiley (1998).

Sen, P. C., *Principles of Electric Machines and Power Electronics*, John Wiley & Sons, Inc. (1989).

Shuzo, O., "Distillation Engineering," Translated by Technology Promotion association (Thailand Japan), Bangkok (1993).

Smith, J. M., Van ness, Abbott, M. M., *Introduction to Chemical Engineering Thermodynamic*, 6th edition, McGraw-Hill (2001).

Van Wylen, G. J., *Thermadynamics*, John Wiley & Sons, Inc. (1959).

Vielstich, W., Lamm, A. and Gasteiger, H. A., *Handbook of Fuel Cells Fundamentals Technology and Applications*, Volume 4, John Wiley & Sons Inc., USA (2003).

Warren, L. M., Julian, C. S. and Peter Harriott, *Unit Operations of Chemical Engineering*, 4th edition, McGraw-Hill, Inc. (1993).

Williams, K. R., *An Introduction to Fuel Cells*, Elsevier publishing Company (1966).

Yoo, K. P., Lee, K. S., Lee, W. H. and Park, H. S., "Diagnosis of Thermodynamic Efficiency in Heat Integrated Distillation," *Korean J. Chem. Eng.*, **5**, 123 (1988).

Yun, Y. and Yoo, Y. D., "Performance of a Pilot-Scale Gasifier for Indonesian Baiduri Coal," *Korean J. Chem. Eng.*, **18**, 679 (2001).

Catalysis Letters Vol. 100, Nos. 3–4, April 2005 (© 2005)
DOI: 10.1007/s10562-004-3445-6

Role of titania in TiO_2–SiO_2 mixed oxides-supported metallocene catalyst during ethylene/1-octene copolymerization

Bunjerd Jongsomjit*, Sutti Ngamposri, and Piyasan Praserthdam

Department of Chemical Engineering, Faculty of Engineering, Center of Excellence on Catalysis and Catalytic Reaction Engineering, Chulalongkorn University, Bangkok, 10330, Thailand

Received 29 September 2004; accepted 11 December 2004

The present study showed enhanced activities of ethylene/1-octene copolymerization via TiO_2–SiO_2 mixed oxides-supported MAO with a zirconocene catalyst. It was proposed that titania was decorated on silica surface and acted as a spacer to anchor MAO to the silica support resulting in less steric hindrance and less interaction on the support surface.

KEY WORDS: mixed oxides; silica; supported catalyst; titania; zirconocene catalyst.

1. Introduction

Because of the commercial interest of using metallocene catalysts for olefin polymerization, it has led to an extensive effort for utilizing metallocene catalysts more efficiently. It is known that the copolymerization of ethylene with higher 1-olefins is a commercial importance for productions of elastomer and linear low-density polyethylene (LLDPE). Metallocene catalysts with MAO have been studied for such a copolymerization. In fact, zirconocene catalysts along with MAO have been reported for a potential use to polymerize ethylene with 1-olefins [1–2].

However, it was found that homogeneous metallocene catalytic system has two major disadvantages; the lack of morphology control of polymers produced and reactor fouling. Therefore, binding these metallocene catalysts onto inorganic supports can provide a promising way to overcome these drawbacks. It has been reported that many inorganic supports such as SiO_2, Al_2O_3, and $MgCl_2$ have been extensively studied [3–13]. It has been mentioned that silica is perhaps the most widely used support for metallocene catalysts so far. Unfortunately, due to the support effect, it is found that the catalytic activity of catalysts in heterogeneous system is usually lower than the homogeneous one. Therefore, a modification of the support properties is required in order to maintain high activity as in the homogeneous system or even closer. TiO_2–SiO_2 mixed oxide has been considered to be very attractive as catalysts and supports, which have brought much attention in recent years. It was reported that TiO_2–SiO_2mixed materials have been used as catalysts and supports for various reactions [14]. This TiO_2–SiO_2 mixed oxide would lead to robust catalytic supports of metallocene catalysts for olefin polymerization.

In this present study, the ethylene/1-octene copolymerization using TiO_2–SiO_2 mixed oxides supported-MAO with a zirconocene catalyst was investigated for the first time. The ratios of TiO_2/SiO_2 used were varied. The mixed oxide supports and catalyst precursors were prepared, characterized and tested for ethylene/1-octene copolymerization. The role of TiO_2 in the mixed oxide supports was also further discussed.

2. Experimental

All chemicals [TiO_2 (anatase, Ishihara), SiO_2 (Cariact P-10), toluene, rac-ethylenebis (indenyl) zirconium dichloride [$Et(Ind)_2ZrCl_2$], methylaluminoxane (MAO), trimethylaluminum (TMA) and 1-octene] were manipulated under an inert atmosphere using a vacuum glove box and/or Schelenk techniques.

2.1. Materials

2.1.1. Preparation of TiO_2–SiO_2 mixed oxides support

TiO_2–SiO_2 mixed oxide supports [surface areas of SiO_2 = 300 $m^2\ g^{-1}$ and TiO_2 (anatase form) = 70 $m^2\ g^{-1}$] for MAO were prepared according to the method described by Conway *et al.* [15]. The TiO_2:SiO_2 ratios were varied from 0:1, 2:8, 4:6, 6:4, 8:2, and 1:0. The supports were heated under vacuum at 400 °C for 6 h.

2.2. Preparation of TiO_2–SiO_2 mixed oxides-supported MAO

One gram of the TiO_2–SiO_2 mixed oxide support obtained from 2.1.1 was reacted with the desired amount of MAO at room temperature and stirred for

* To whom correspondence should be addressed.
E-mail: bunjerd.j@chula.ac.th

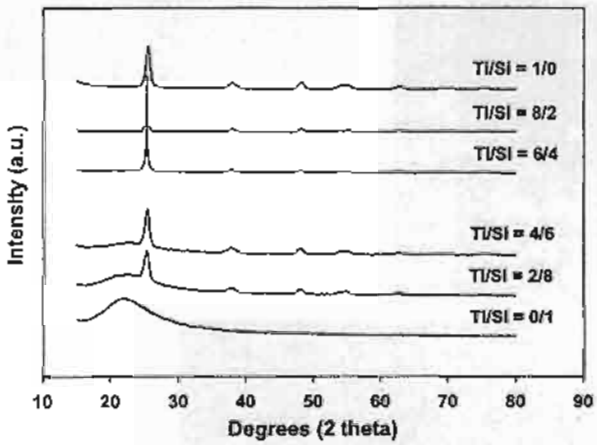

Figure 1. XRD patterns of various TiO_2–SiO_2 mixed oxide supports before MAO impregnation.

30 min. The solvent was then removed from the mixture. About 20 mL of toluene was added into the obtained precipitate, stirred the mixture for 5 min, and then removed the solvent. This procedure was done for 5 times to ensure the removal of impurities. Then, the solid part was dried under vacuum at room temperature to obtain white powder of TiO_2–SiO_2 mixed oxides-supported MAO.

2.3. Polymerization

The ethylene/1-octene copolymerization reaction was carried out in a 100 mL semi-batch stainless steel autoclave reactor equipped with a magnetic stirrer. At first, 0.1 g of the supported MAO ($[Al]_{MAO}/[Zr]$ = 1135) and 0.018 mol of 1-octene along with toluene (to make the total volume of 30 mL) were put into the reactor. The desired amount of $Et(Ind)_2ZrCl_2$ (5×10^{-5} M) and TMA ($[Al]_{TMA}/[Zr]$ = 2500) was mixed and stirred for 5-min aging at room temperature, separately, then was injected into the reactor. The reactor was frozen in liquid nitrogen to stop reaction for 15 min and then the reactor was evacuated to remove argon. The reactor was heated up to polymerization temperature (70 °C). By feeding the fixed amount of ethylene (0.018 mol ~6 psi) into the reaction mixtures, the ethylene consumption can be observed corresponding to the ethylene pressure drop. The polymerization reaction was stopped and the reaction time used was recorded when all ethylene

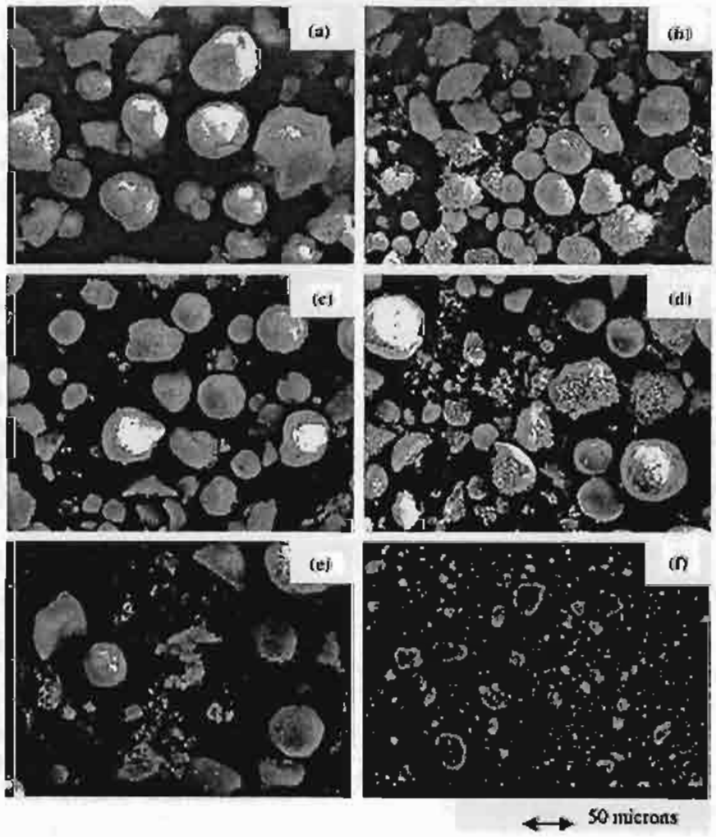

Figure 2. SEM micrographs of various TiO_2–SiO_2 mixed oxide supports before MAO impregnation: (a) Ti/Si = 0/1, (b) Ti/Si = 2/8, (c) Ti/Si = 4/6, (d) Ti/Si = 6/4, (e) Ti/Si = 8/2, (f) Ti/Si = 1/0.

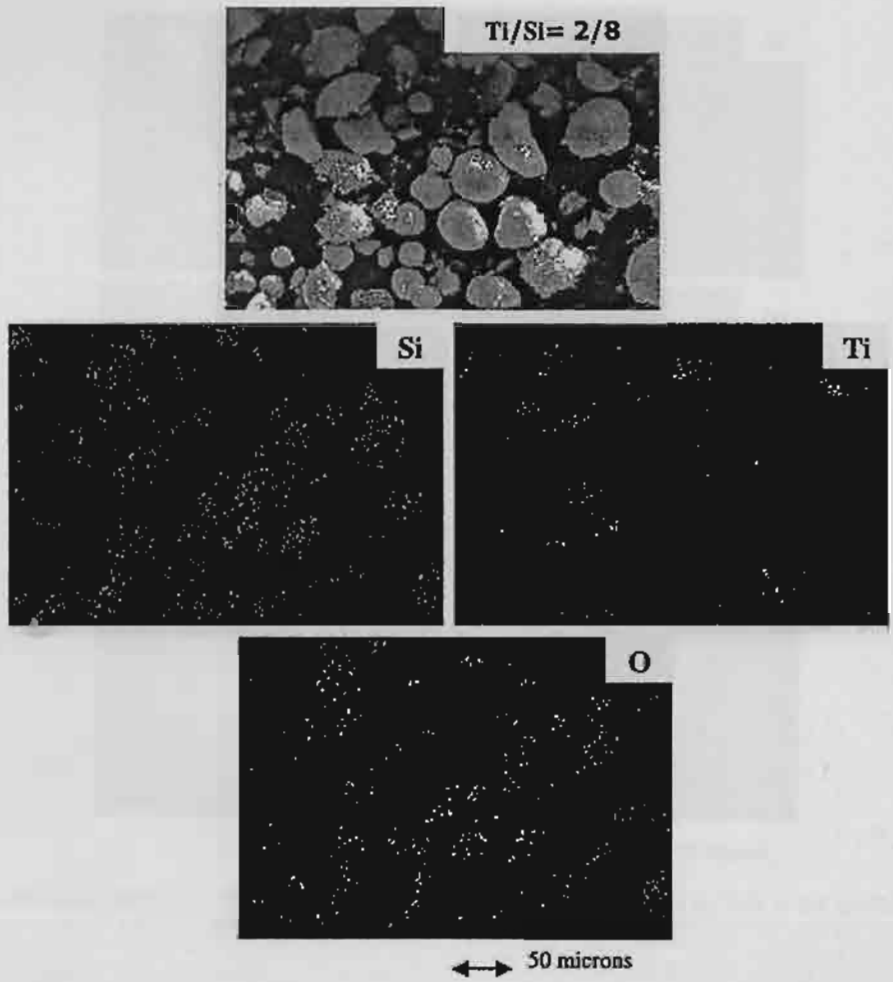

Figure 3. EDX mapping of a typical TiO_2–SiO_2 mixed oxide supports before MAO impregnation.

(0.018 mol) was totally consumed. To start reaction, 0.018 mol of ethylene was fed into the reactor containing the comonomer and catalyst mixtures. After all ethylene was consumed, the reaction was terminated by addition of acidic methanol (0.1% HCl in methanol) and stirred for 30 min. After filtration, the obtained copolymer (white powder) was washed with methanol and dried at room temperature.

2.4. Characterization

2.4.1. Characterization of supports and catalyst precursors

X-ray diffraction: XRD was performed to determine the bulk crystalline phases of samples. It was conducted using a SIEMENS D-5000 X-ray diffractometer with CuK_α(λ = 1.54439 Å). The spectra were scanned at a rate of 2.4° min^{-1} in the range 2θ = 20–80°.

Scanning electron microscopy and energy dispersive X-ray spectroscopy: SEM and EDX were used to determine the sample morphologies and elemental distribution throughout the sample granules, respectively. The SEM of JEOL mode JSM-5800LV was

Table 1
Catalytic activities during ethylene/1-octene copolymerization via TiO_2–SiO_2 mixed oxides supported-MAO with zirconocene catalyst

TiO_2–SiO_2 Weight ratios	wt% of TiO_2 in mixed support	Polymer yield (g)	Polymerization time (s)	Catalytic activity[a] ($\times 10^{-4}$ kg polymer mol^{-1} Zr. h)
Homogeneous	0	1.13	87	3.1
0/100	0	1.19	152	1.9
20/80	20	1.14	116	2.4
40/60	40	1.19	132	2.2
60/40	60	1.18	149	1.9
80/20	80	1.17	157	1.8
100/0	100	1.13	161	1.7

[a]Activities were measured at polymerization temperature of 70 °C, [ethylene] = 0.018 mol, [1-octene] = 0.018 mol, $[Al]_{MAO}/[Zr]$ 1135, $[Al]_{TMA}/[Zr]$ = 2500, in toluene with total volume = 30 mL, and [Zr] = 5×10^{-5} M.

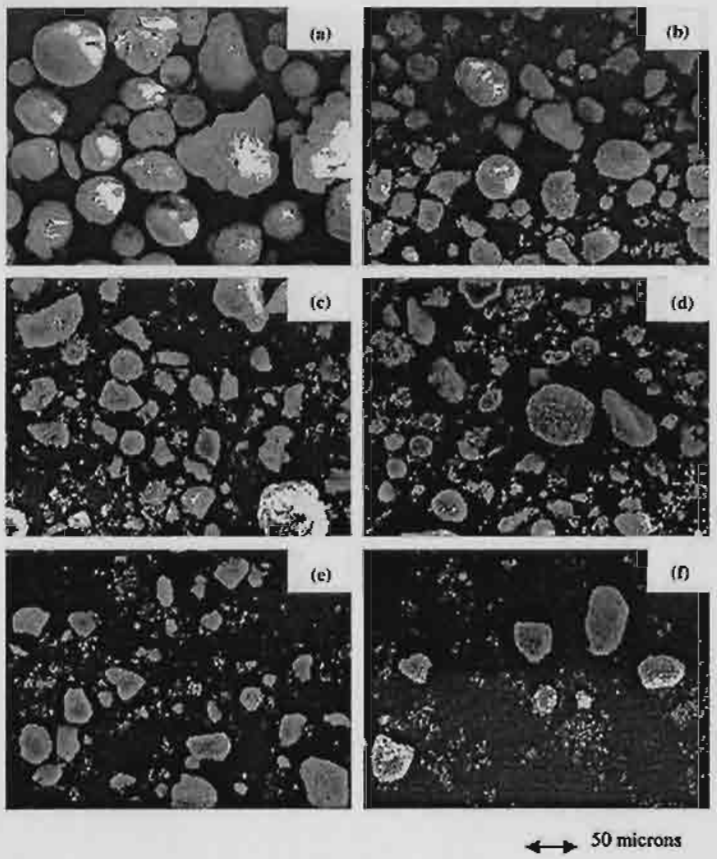

Figure 4. SEM micrographs of various TiO_2–SiO_2 mixed oxide supports after MAO impregnation; (a) Ti/Si = 0/1, (b) Ti/Si = 2/8, (c) Ti/Si = 4/6, (d) Ti/Si = 6/4, (e) Ti/Si = 8/2, (f) Ti/Si = 1/0.

applied. EDX was performed using Link Isis series 300 program.

FTIR spectroscopy: FTIR was conducted on a Perkin-Eelmer series 2000 instruments. The supports (1 mg) were mixed with 100 mg dried KBr. The sample cell was purged with oxygen. About 400 scans were accumulated for each spectrum in transmission with a resolution of 4 cm^{-1}. The spectrum of dried KBr was used as a background subtraction.

2.4.2. Characterization of polymer

Scanning electron microscopy: SEM was performed to study morphologies of polymers produced. The same equipment as mentioned above was employed.

Gel permeation chromatography (GPC): A high temperature GPC (Waters 150-C) equipped with a viscometric detector, differential optical refractometer and four Styragel HT type columns (HT3, HT4, HT5, and HT6) with a 1×10^7 exclusion limit for polysyrene was used to determined the molecular weight and molecular weight distributions of the copolymers produced. The analyses were performed at 135 °C using 1,2,4-trichlorobenzene as the solvent. The columns were calibrated with standard narrow molecular weight distribution polystyrene and LLDPE.

3. Results and discussion

The present study showed influences of TiO_2–SiO_2 mixed oxide supports on catalytic activities in heterogeneous metallocene catalytic system. The mixed oxide supports containing various amounts of titania and silica were characterized before and after impregnation with MAO. XRD patterns of the supports before impregnation with MAO are shown in figure 1. It was observed that the pure silica exhibited a broad XRD peak assigning to the conventional amorphous silica. Similar to the pure silica, the XRD patterns of the pure titania indicated only the characteristic peaks of anatase titania at 25° (major), 37°, 48°, 55°, 56°, 62°, 71°, and 75°. XRD patterns of the mixed oxide supports containing various amounts of titania and silica revealed the combination of titania and silica supports based on their content. It can be seen that the intensity of XRD characteristic peaks for both supports was changed based on the ratios of TiO_2/SiO_2. After impregnation with MAO, the mixed oxide supports were again identified using

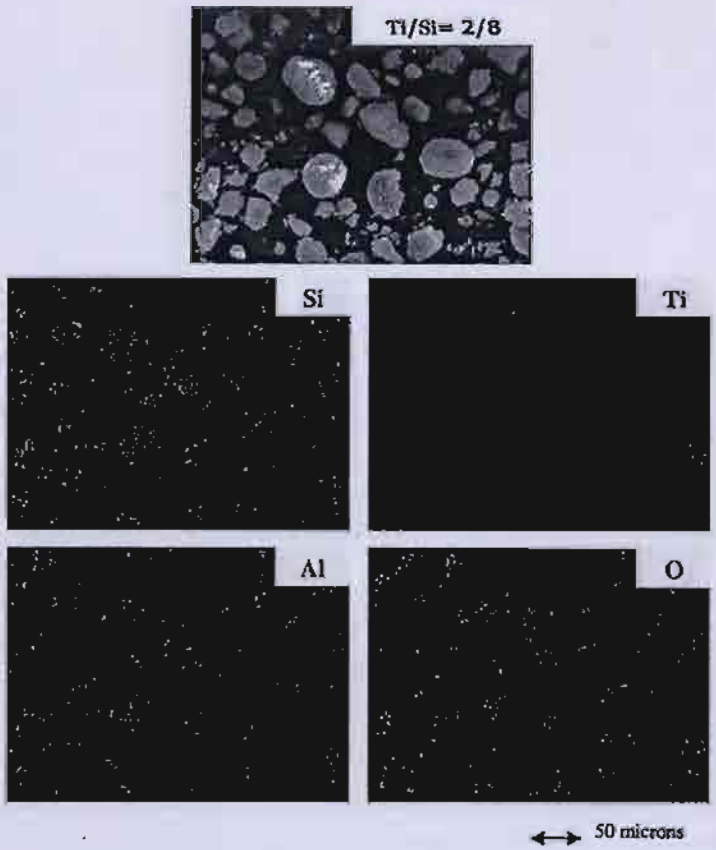

Figure 5. EDX mapping of a typical TiO_2–SiO_2 mixed oxide supports after MAO impregnation.

XRD. It was found that XRD patterns for the supports after impregnation with MAO were identical with those before impregnation with MAO indicating highly dispersed MAO species. In order to determine the morphologies and elemental distributions of the supports before and after impregnation, SEM and EDX were performed, respectively. The SEM micrographs of the supports before impregnation with MAO were shown in figure 2. It showed that silica was appeared in larger particles than titania. It also indicated that at the low content of titania ranged between 20 and 60%, titania was found to decorate on the silica surface as seen in the SEM micrographs. However, at high content of titania, it revealed that titania, essentially isolated from the silica surface. This was probably because the adsorption ability of silica surface with titania was limited by the titania contents in the mixed oxide supports. The distribution of all elements (Si, Ti, and O) obtained from EDX was similar in all samples. The typical EDX mapping images for the mixed oxide support are shown in figure 3 indicating titania located on the silica outer surface. After impregnation with MAO, SEM and EDX of the supports were also conducted. The SEM micrographs of the supports after impregnation with MAO are shown in figure 4 indicating similar results as seen in figure 2. The EDX mapping images of the supports can provide more information about the distribution of MAO as seen for Al distribution mapping on each support. It was found that MAO was well distributed all over the support granules. The typical EDX mapping images for the mixed oxide supports after impregnation with MAO are shown in figure 5. Figure 6 apparently shows SEM and EDX mapping of titania located on the outer surface of silica support. IR spectroscopy was also performed in order to identify chemical species and bonding of the mixed oxide supports. The IR spectra of samples are shown in figure 7. It revealed that at low concentrations of titania, the IR band at ca. 980 cm^{-1} assigning to Si–O–Ti connectivity was observed as also reported by Dutoit *et al.* [16]. The strong IR bands were also seen at ca. 1100 cm^{-1} assigning to asymetric Si–O–Si stretching vibration. Then, the various TiO_2–SiO_2 mixed oxide supports after impregnation with MAO were used and investigated for catalytic activities. Copolymerization of ethylene/1-octene via various TiO_2–SiO_2 mixed oxides-supported MAO with zirconocene catalyst was performed in order to determine the catalytic activities influenced by the various supports. The resulted reaction study is shown in table 1 and figure 8. The activities of the supported system were much

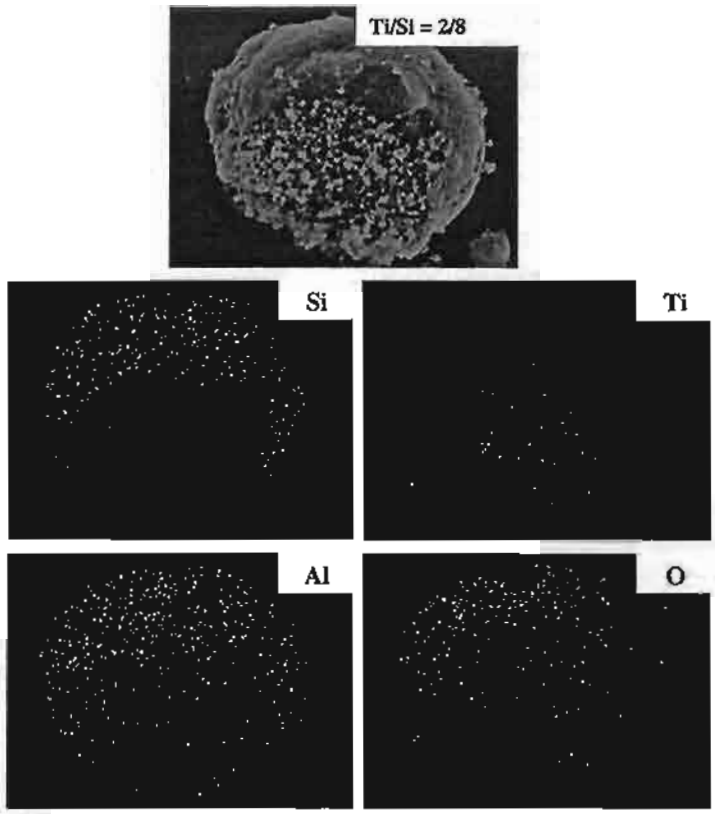

Figure 6. SEM and EDX mapping of titania located on the mixed support granule.

lower than the homogeneous one as expected. However, considering only the supported system, it was found that activities dramatically increased with increasing the amounts of titania up to 60% in the supports compared with those for the pure silica support. The maximum activity can be obtained with the presence of 20% titania in the mixed support. However, with increasing the amounts of titania more than 60% resulted in lower activities compared to the pure silica. It was also found that the activity for the pure titania is the lowest because the strong support interaction [17] between MAO and titania was more pronounced. Based on the resulted activities, the role of titania in TiO_2–SiO_2 mixed oxide supports can be proposed. In order to give a better understanding for the role of titania, a conceptual model for titania effect is illustrated in Scheme 1. As known,

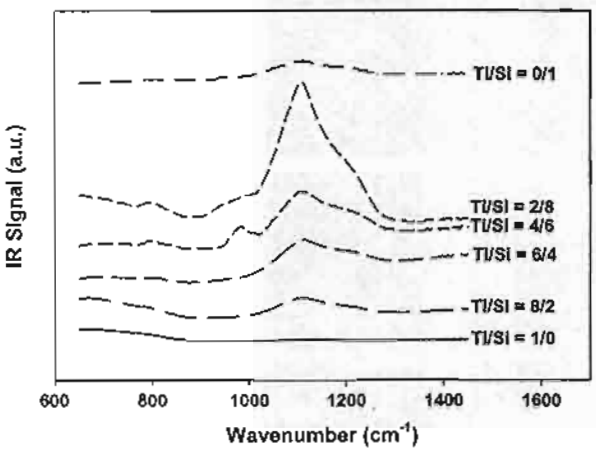

Figure 7. IR spectra of various mixed oxide supports.

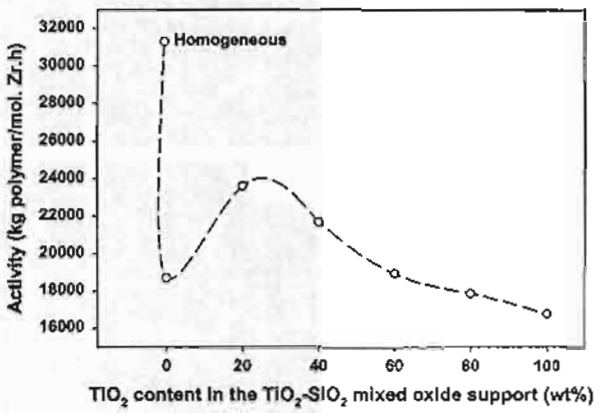

Figure 8. Activities of ethylene/1-octene copolymerization via various TiO_2–SiO_2 mixed oxides-supported MAO with a zirconocene catalyst.

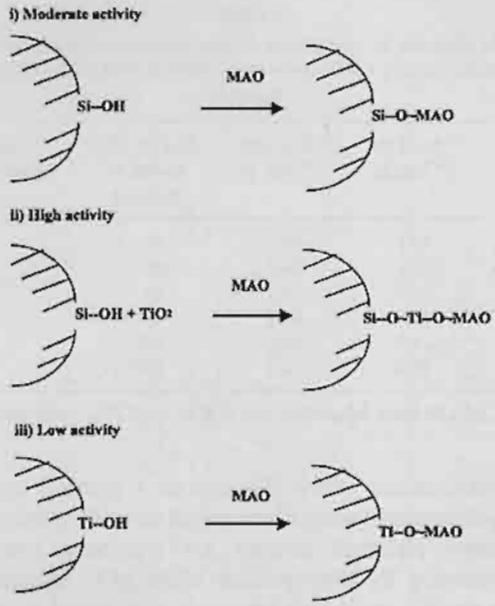

Scheme 1. A conceptual model for evaluation of activities via various TiO_2–SiO_2 mixed oxide supports.

when the heterogeneous system was conducted, activities decreased significantly compared to the homogeneous one as also seen in figure 8. This should be due to a loss of active species by support interaction and/or the steric hindrance arising from the support. Considering Scheme 1, activities on the heterogeneous system can be divided into three levels; (i) moderate activity with the conventional pure silica support, (ii) high activity with the certain amounts of titania present in the mixed oxide support, (iii) low activity with the pure titania support (due to strong support interaction [17]). In Scheme 1 (ii), it showed that the presence of certain amounts (20–60 wt%) of titania dramatically enhanced activities. The contribution of titania can be drawn as MAO anchored on silica with titania as a spacer group. It can be also seen from SEM and EDX that at low content of titania, it was apparently decorated on silica surface and acted as a spacer to anchor MAO to the silica support. Thus, activities increased about 15–25% with the presence of titania between 20 and 40% in the mixed oxide supports. It should be mentioned that increased activities with the presence of titania as a spacer were observed because of less steric hindrance and less interaction on the support surface when a spacer was introduced. Thus, this was suggested to be more homogeneous-like system. Investigation of a spacer such as silane in copolymerization of ethylene/1-olefins was also reported [18,19]. However, when high amounts of titania were added, activities decreased because the strong support interaction as seen in Scheme 1 (iii) can occurred resulting in a combination

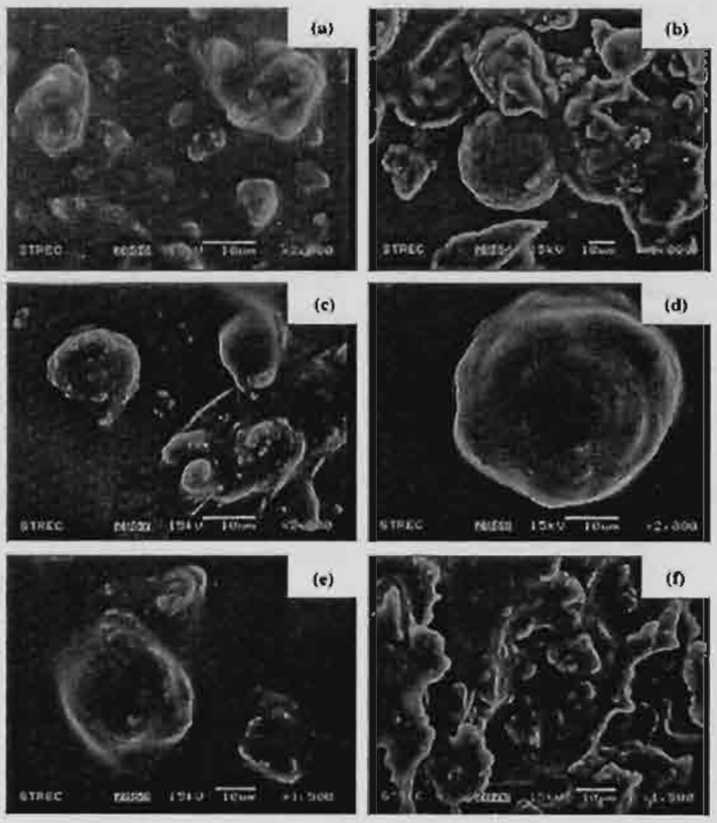

Figure 9. SEM micrographs of polymers obtained with various TiO_2–SiO_2 mixed oxide supports; (a) Ti/Si = 0/1, (b) Ti/Si = 2/8, (c) Ti/Si = 4/6, (d) Ti/Si = 6/4, (e) Ti/Si = 8/2, (f) Ti/Si = 1/0.

Table 2
Molar weight and molecular weight distribution of polymers obtained via TiO_2–SiO_2 mixed oxides supported-MAO with zirconocene catalyst

TiO_2–SiO_2 weight ratios	wt% of TiO_2 in mixed support	M_w^a ($\times 10^{-4}$ g mol^{-1})	M_n^a ($\times 10^{-4}$ g mol^{-1})	MWD[a]
0/100	0	3.61	1.06	3.4
20/80	20	3.42	1.08	3.2
40/60	40	2.91	1.13	2.6
60/40	60	2.60	0.96	2.7
80/20	80	2.65	0.93	2.8
100/0	100	2.41	0.59	4.1

[a]Obtained from GPC and MWD was calculated from M_w/M_n.

between Scheme 1 (i) and (iii) where titania started to isolate from silica as segregated titania. Morphologies of polymers produced via various supports were also investigated. The SEM micrographs of polymers are shown in figure 9. It indicated that there was no significant change in polymer morphologies upon various mixed oxide supports used. The molecular weight based on weight average (M_w) and based on number average (M_n), and molecular weight distribution (MWD) of polymers obtained are shown in table 2. It indicated that the addition of TiO_2 resulted in decreased molecular weights of polymers compared to those of pure SiO_2. However, the narrower molecular weight distribution was observed with the addition of TiO_2 except for the one with pure TiO_2.

4. Conclusions

The present study revealed influence of various TiO_2–SiO_2 mixed oxides supported-MAO on the catalytic activities during copolymerization of ethylene/1-octene. It was found that at certain contents of titania ranged between 20 and 60 wt% in the mixed oxide support, activities dramatically increased by 15–25% compared to those with the conventional pure silica support. It was proposed that titania added acted as a spacer to anchor MAO to the silica support resulting in less steric hindrance and less interaction on the support surface. However, larger amounts of titania resulted in lower activities because the strong support interaction between titania and MAO was more pronounced. The molecular weights of polymers were found to decrease with the addition of TiO_2 whereas narrower molecular weight distribution can be observed in the mixed TiO_2–SiO_2 supports.

Acknowledgments

The authors would like to thank the Thailand Research Fund (TRF), the National Research Council of Thailand (NRCT) and Thailand–Japan Transfer Technology Project (TJTTP-JBIC) for the financial support of this work. We would like to extend our thankful to Professor Takeshi Shiono at Hiroshima University, Japan for his kind advice of this project.

References

[1] C.L.P Shan, J.B.P Soares and A Penlidis, Polym. Chem. 40 (2002) 4426.
[2] K.J Chu, C.L.P Shan, A Soares and J.B.P Penlidis, Macromol. Chem. Phys. 200 (1999) 2372.
[3] A.M Uusitalo, T.T Pakkanen and E.I Iskola, J. Mol. Catal. A: Chem. 177 (2002) 179.
[4] K Soga and M Kaminaka, Makromol. Chem. 194 (1993) 1745.
[5] Y.S Ko, T.K Han, J.W Park and S.I Woo, Macromol. Rapid Commun. 17 (1996) 749.
[6] T. Sugano and K. Yamamoto *Eur. Pat. Appl.* 728773 (1996).
[7] M Margue and A Conte, J. Appl. Polm. Sci. 86 (2002) 2054.
[8] S Sensarma and S Sivaram, Polym. Inter. 51 (2002) 417.
[9] P.G Belelli, M.L Ferreira and D.E Damiani, Appl.Catal. A: Gen. 228 (2002) 189.
[10] J.T Xu, Y.B Zhu, Z.Q Fan and L.X Feng, J. Polym. Sci. Part A: Polym. Chem. 39 (2001) 3294.
[11] L Korach and K Czaja, Polym. Bull. 46 (2001) 67.
[12] A Koppl and H.G Alt, J. Mol. Catal. A: Chem. 165 (2001) 23.
[13] B Jongsomjit, P Praserthdam and P Kaewkrajang, Mater. Chem. Phys. 86 (2004) 243.
[14] X Gao and I.E Wachs, Catal. Today 51 (1999) 233.
[15] S.J Conway, J.W Falconer and C.H Rochester, J. Chem. Soc. Faraday Trans. 185 (1989) 71.
[16] D.C.M Dutoit, M Schneider and J Baiker A., J. Catal. 153 (1995) 165.
[17] R Riva, H Miessuer, R Vitali and G Del Piero, Appl. Catal. A 196 (2000) 111.
[18] C Chao, W Pratchayawutthirat, P Praserthdam Shiono and T Rempel, Macromol. Rapid Commun. 23 (2002) 672.
[19] B Jongsomjit, P Kaewkrajang, S.E Wanke and P Praserthdam Catal. Lett. 94 (2004) 205.

Jointly published by
Akadémiai Kiadó, Budapest
and Springer, Dordrecht

React.Kinet.Catal.Lett.
Vol. 85, No. 2, 299-304
(2005)

RKCL4652

METAL-SUPPORT INTERACTION IN MESOPOROUS SILICA SUPPORTED COBALT FISCHER-TROPSCH CATALYSTS

Joongjai Panpranot*, Sujaree Kaewgun and Piyasan Praserthdam
Center of Excellence on Catalysis and Catalytic Reaction Engineering,
Department of Chemical Engineering, Chulalongkorn University, Bangkok, Thailand

Received September 14, 2004
In revised form December 14, 2004
Accepted December 16, 2004

Abstract

The pore structure of silica supports (SiO_2 or MCM-41) has little influence on the metal-support interaction in silica supported cobalt catalysts. Cobalt dispersion, reduction behavior, and catalytic properties for the Fischer-Tropsch synthesis were primarily affected by the metal particle size.

Keywords: Cobalt catalyst, metal-support interaction, mesoporous silica, CO hydrogenation

INTRODUCTION

Cobalt-based catalysts are widely used in CO hydrogenation or Fischer-Tropsch synthesis (FTS) especially when high molecular weight paraffins are preferred [1-2]. To increase their activity, cobalt is usually deposited on a high surface area oxide support to obtain a high metal dispersion. Recently, the use of high surface area ordered mesoporous materials such as MCM-41 and SBA-15 for preparing Co-based Fischer-Tropsch catalysts has been explored [3-7]. Compared to amorphous silica-supported catalysts with similar Co loading, Co supported on these mesoporous materials have shown higher FTS activity due to a better dispersion of cobalt in mesoporous structure [8]. However, stronger interaction of cobalt species and the support in these catalysts were often found, resulted in catalysts with lower reducibilities. In this study, the effects of pore structure (SiO_2 and MCM-41) and the metal particle size on the metal-support interaction in supported Co F-T catalysts were investigated.

*Corresponding author. Tel: (66)-2-218-6859; Fax: (66)-2-218-6877
E-mail: joongjai.p@eng.chula.ac.th

0133-1736/2005/US$ 20.00.

EXPERIMENTAL

Catalyst preparation

Pure silica MCM-41 was prepared in the same manner as that of Kruk *et al.* [9] using the following gel composition: (1.0 SiO_2): (0.317 TMAOH): (0.45 CTMABr): (66.7 H_2O), where TMAOH denotes tetramethylammonium hydroxide and CTMABr denotes cetyltrimethyl ammonium bromide. High surface area SiO_2 with similar pore size to MCM-41 were obtained from Grace Davison Company. The series of supported Co catalysts (MCM-41 and SiO_2-supported) were prepared by the incipient wetness impregnation of the supports with an aqueous solution containing the desired amount of different cobalt precursors such as cobalt nitrate (Aldrich), cobalt acetate (APS), cobalt acetylacetonate (Aldrich), and cobalt chloride (Fluka). The catalysts were dried overnight in an oven at 110°C and then were calcined at 500°C in an air flow for 2 h. Elemental analysis was carried out for all the catalysts after calcination. The cobalt loading was determined to be approximately 7-8 wt.%.

Catalyst characterization

The BET surface area, pore volume, average pore diameter, and pore size distribution of the catalysts were determined by N_2 physisorption using a Micromeritics ASAP 2000 automated system. Each sample was degassed in the Micromeritics ASAP 2000 at 150°C for 4 h prior to N_2 physisorption. The XRD spectra of the catalysts were measured using a SIEMENS D5000 X-ray diffractometer, using Cu Kα radiation with a Ni filter in the 2-8° or 10-80°2θ angular regions. Temperature programmed reduction was performed using an in-house system and a temperature ramp of 5°C/min from 30 to 300°C in a flow of 5% H_2 in argon. Approximately 0.20 g of a calcined catalyst was placed in a quartz tube in a temperature-controlled oven and connected to a thermal conductivity detector. The H_2 consumption was measured by analyzing the effluent gas with a TCD.

Reaction study

CO hydrogenation was carried out at 220°C and 1 atm total pressure in a fixed-bed stainless steel reactor under differential conversion conditions. A flow rate of H_2/CO/Ar = 20/2/8 cm^3/min was used. Typically, 0.2 g of the catalyst samples was reduced *in situ* in flowing H_2 (50 cc/min) at 350°C for 10 h prior to reaction. The product samples were taken at 1-h intervals and

analyzed by gas chromatography. Steady state was reached after 6 h time-on-stream in all cases.

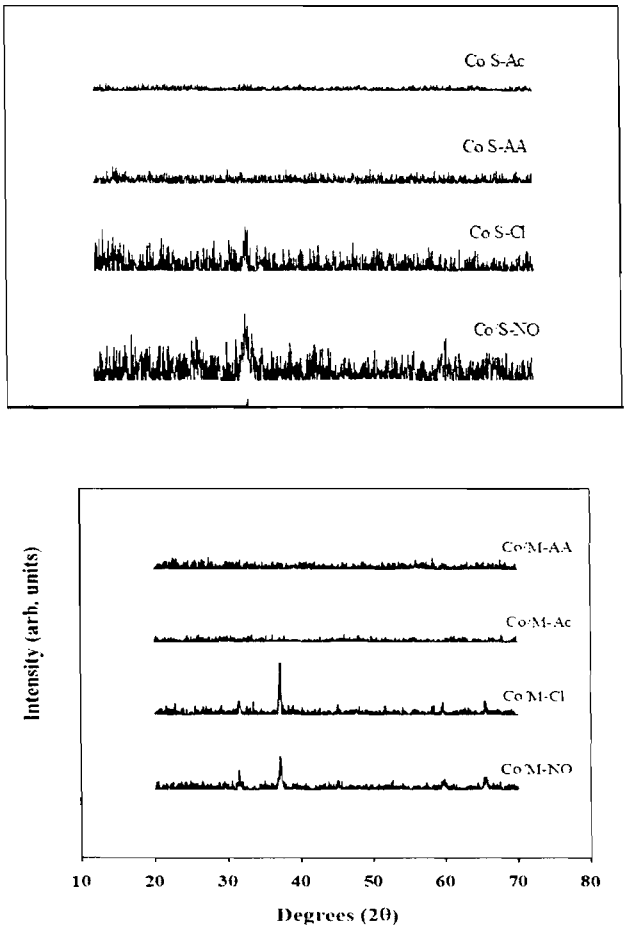

Fig. 1. XRD patterns of different SiO_2 and MCM-41-supported Co catalysts

RESULTS AND DISCUSSION

Two types of silica supported Co catalysts (Co/SiO_2 and Co/MCM-41) have been prepared using the incipient wetness impregnation method in order to study the effect of pore size and pore structure of the supports on cobalt dispersion, reduction behavior, and catalytic properties for the Fischer-Tropsch synthesis (FTS). The BET surface areas, pore volumes, and average pore

diameters of the original supports and the catalysts are given in Table 1. The significant decrease in surface area of the original support material suggests that cobalt was deposited in some of the pores of the supports. The XRD patterns of SiO_2 and MCM-41 supported Co catalysts after calcination in air at

Table 1

Characteristics of SiO_2 and MCM-41 supported Co catalysts

Catalyst	Co (wt%)[a]	BET S.A.[b] (m^2/g)	d_P[c] Co_3O_4 (nm)
SiO_2	-	717	-
Co/S-Ac	7.9	562	n/a
Co/S-AA	7.7	595	n/a
Co/S-Cl	7.1	517	17.6
Co/S-NO	8.4	571	16.4
MCM-41	-	1234	-
Co/M-Ac	8.3	756	n/a
Co/M-AA	7.8	675	n/a
Co/M-Cl	7.1	646	15.0
Co/M-NO	8.1	747	6.3

[a] Based on atomic absorption spectroscopy of the calcined catalysts.
[b] Based on the calcined catalysts. Error of measurement = ± 10%.
[c] Based on XRD line broadening of the calcined catalysts

500°C for 2 h are shown in Fig. 1. The catalysts prepared from cobalt nitrate and cobalt chloride exhibited the diffraction peaks of at 2θ of *ca.* 31.3°, 36.8°, 45.1°, 59.4°, and 65.4°, indicating the presence of Co_3O_4. The catalysts prepared from organic precursors (cobalt acetate and cobalt acetyl acetonate did not exhibit any distinct XRD patterns. This suggests that the crystallite sizes of Co_3O_4 prepared from organic precursors were much smaller than those prepared form inorganic ones [10].

Temperature-programmed reduction (TPR) profiles of SiO_2- and MCM-41-supported Co catalysts are shown in Fig. 2. In general, the reduction of Co_3O_4 composes of the two-step reduction of Co_3O_4 to CoO and then to Co^0 [11,12]. TPR profiles for supported Co catalysts, however, are more complex than for bulk Co_3O_4 due to various causes such as variation in metal particle size, metal-support interaction, and support porous structure resulting in differently reducible cobalt species on the support [13-14]. The TPR profiles of silica supported Co catalysts used in this study were found to be dependent on the type of cobalt precursors. Using organic cobalt precursors such as cobalt